Thesis

For the Degree of Master of Science

NMR Backbone Assignment of Fibronectin Extradomain B in the Free State and in Complex with the Specific Binding Aptide

핵자기공명분광법을 이용한 EDB와

EDB–앱타이드 복합체의 backbone assignment

February, 2014

By

Seung Ah Shin

Graduate School of Agriculture Biotechnology

Seoul National University

NMR Backbone Assignment of Fibronectin Extradomain B in the Free State and in Complex with the Specific Binding Aptide

핵자기공명분광법을 이용한 EDB와
EDB–앱타이드 복합체의 backbone assignment

지도교수 윤철희

이 논문을 이학 석사학위논문으로 제출함

2014 년 2 월

서울대학교 대학원
농생명공학부 바이오모듈레이션 전공
신승아

신승아의 석사학위논문을 인준함

2014 년 1 월

위 원 장 석 차 옥 (인)

부 위 원 장 서 정 용 (인)

위 원 윤 철 희 (인)

ABSTRACT

NMR Backbone Assignment of Fibronectin Extradomain B in the Free State and in Complex with the Specific Binding Aptide

Seung-Ah Shin
Major in Biomodulation
Graduate School of Agriculture Biotechnology
Seoul National University

The extra domain B (EDB) of fibronectin, a naturally occurring marker of tissue remodeling and angiogenesis, is expressed in the majority of aggressive solid human tumors, whereas it is not detectable in normal vessels and tissues. Aptides based on the tryptophan zipper scaffold with variable target-binding arms were shown to recognize diverse target proteins with high affinity and specificity. I employed NMR spectroscopy in order to characterize the binding mode of EDB and its specific aptide.

Performed three-dimensional triple resonance NMR experiments to assign the backbone resonances of free EDB and EDB:aptide complex using double labeled ($^{13}C/^{15}N$) and triple labeled ($^{2}H/^{13}C/^{15}N$) samples. 3D CBCACONH, HNCACB, and HBHA(CO)NH were recorded and analyzed, yielding a total of 97% of the $^{1}H\alpha$, $^{13}C\alpha$,

and $^{13}C\beta$ chemical shift assignment. After that I calculated the Chemical Shift Index (CSI) using the backbone chemical shifts.

The results indicated that six β-strand secondary structures were found between residues 5-15, 20-28, 34-42, 51-55, 62-64, and 72–80 and also a α-helical turn between residues 56–59. Comparison of the CSI between free EDB and the EDB:aptide complex revealed a dramatic change in the secondary structures upon the complex formation. Based on the backbone chemical shift assignment, side chain assignment and distance restraint measurement are underway to determine the three-dimensional structure of the complex.

……

Keywords : aptide, backbone assignment, fibronectin extra domain B(EDB), NMR spectroscopy, protein-protein interaction

Student ID : 2012-22623

CONTENTS

LIST OF FIGURES

LIST OF TABLES

ABBREVIATIONS

2D	Two-dimensional
3D	Three-dimensional
CBCA(CO)NH	Correlation spectroscopy for H^N-N^H-$C\alpha^{i-1}$-$C\beta^{i-1}$
CSI	Chemical shift index
IPTG	Isopropyl β-D-1-thiogalactopyranoside
HBHA(CO)NH	Correlation spectroscopy for H^N-N^H-H^α-H^β
HSQC	Heteronuclear single quantum coherence
HNCACB	Correlation spectroscopy for $C\alpha^{i-1}$-$C\beta^{i-1}$- H^N-N^H-$C\alpha^i$-$C\beta^i$
NMR	Nuclear magnetic resonance

Backbone and side chain atoms are denoted as follows:

N^H	Backbone amide nitrogen
H^N	Backbone amide proton
C'	Backbone carbonyl carbon
Cα	Backbone α-carbon
Cβ	Backbone β-carbon
Hα	Backbone α-proton
Hβ	Side chain β-proton

I. INTRODUCTION

1.1. Extra domain B

Angiogenesis generally occurs during the cell development and wound healing process for the tissue repair or regeneration. Unregulated angiogenesis often leads to the induction of tumor, tumor recurrence and also chronic inflammation. During the tumor growth, neovasculature is formed upon the remodeling of extracellular matrix (ECM) through the degradation and synthesis of ECM components. One of the most prominent proteins in the ECM, fibronectin, is a high molecular adhesive glycoprotein, which mediate ECM function such as migration, differentiation, adhesion and proliferation of cells. Under tumor conditions, fibronectin has been shown to undergo alternative splicing to insert the extra domain B (EDB) (Khan ZA *et al.*, 2005) (Fig. 1).

The splice variants of fibronectin with EDB accumulate around the new blood vessels during angiogenesis in malignant tumors, but not around the healthy adult cells. For this reasons, EDB is considered as a biomarker of angiogenesis, which can serve as an appropriate target for tumor diagnosis and therapy.

The 3D-structure of the EDB domain has been solved by NMR spectroscopy in solution in the group of Kurt Wüthrich at the ETH Zurich (PDB entry 2FNB) (Fattorusso R *et al.,* 1999), and is characterized by two antiparallel β sheets that form a β sandwich (Fig. 2). One β sheet is formed by three β strands (A, B, and E), and the other by four β strands (C, C', F and G).

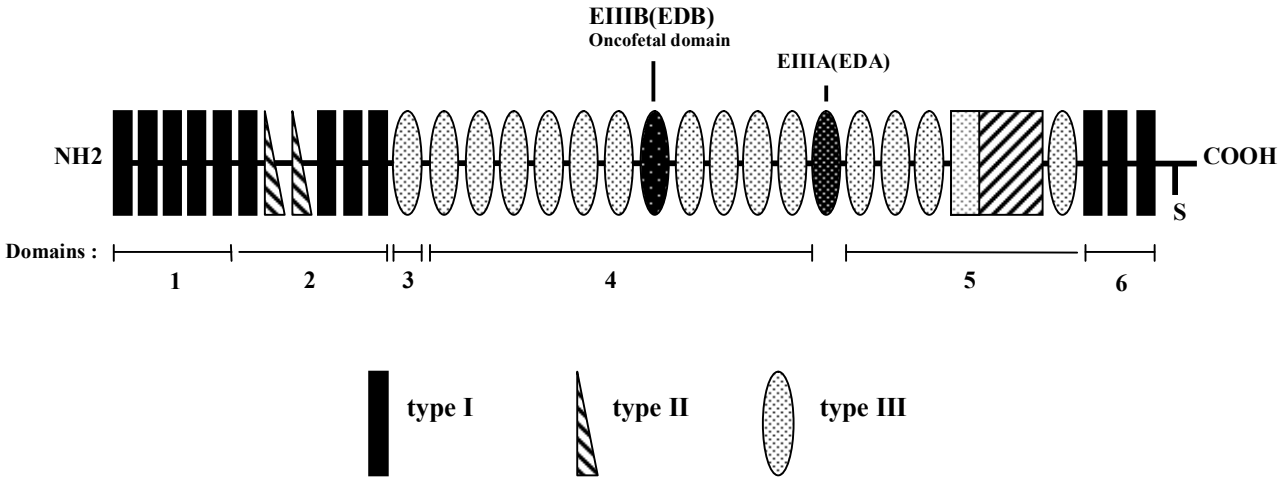

Figure 1. Fibronectin domain structure.

Fibronectin subunit is madeup of a series of repeating units of three different types (type-I, type-II, and type-III). Two subunits are joined by two disulfide bonds at their carboxyl termini. Three repeats can be either inserted or omitted by a mechanism of RNA alternative splicing: EDB, EDA, Domain 5, and Domain 6. Separate functional regions have been identified that contain binding activities for other components of the ECM: domain 1 binds to heparin, DNA, and fibrin; domain 2 binds to gelatin; domain 3 binds to heparin and DNA; domain 4 binds to cells, heparin, and DNA; domain 5 binds to heparin and DNA; domain 6 binds to fibrin.

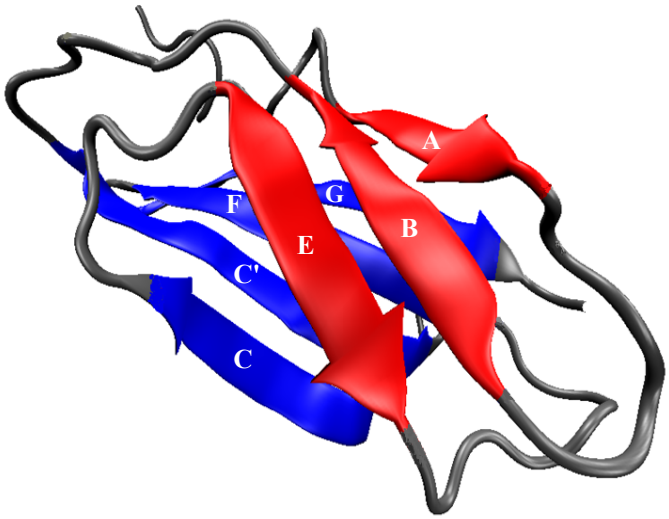

Figure 2. Structure of the EDB domain of fibronectin.

Ribbon drawing of human EDB(PDB entry 2FNB). The two β-sheets formed by three (A, B, E) and four β-strands (C, C', F, G), are colored in red and blue, respectively.

1.2. Aptide

Antibodies have been widely used in a range of biopharmaceutical and biomedical applications due to their intrinsic high affinity and specificity toward various targets. However, poor tissue penetration owing to their large size, undesired effectors functions, immunogenicity, costly recombinant production in mammalian cells, and complex intellectual property barriers have led researchers to seek alternatives to antibodies. Aptamer comprises nucleic acids and proteins that have potential biotechnological applications as an alternative to the immunoglobulin from various biochemical assays. Compared to antibodies, aptamers are much smaller in size but possess similar binding affinity and recognition specificity to their target proteins both *in vitro* and *in vivo.* In this paper, I investigated an artificial high-affinity aptamer-like peptide, an aptide (Kim SY *et al.*, 2011).

Aptides are a novel class of peptide-based molecules that provide a general scaffold of high-affinity and high-specificity against diverse targets. The aptide comprises a β-hairpin scaffold and two target-binding regions. The hairpin scaffold consists of a small (12 amino acids) tryptophan zipper motif that forms a highly stable β-hairpin structure (Fig. 3). The β-hairpin conformation is stabilized by two tryptophan–tryptophan cross-strand pairs that make an edge-to-face interaction (Cochran AG *et al.,* 2001). The target binding regions consist of six amino acids at each end of the hairpin scaffold.

Phage display was used to screen and isolate the specific aptide for EDB that showed high affinity and specificity (Saw PE *et al.*, 2013).After the screening and

affinity maturation, aptides with nanomolar binding affinity against EDB in vitro and specific binding in vivo have been obtained.

Specific aptides against human fibronectin extradomain B (EDB) could be a promising tumor-specific biomarker that can be used in tumor imaging and therapy. The three dimensional structure of the EDB:aptide complex would greatly help to understand how the aptide specifically recognize EDB. As the first step, I carried out the backbone chemical shift assignment of EDB in the free of state and in complex with aptide using a suite of triple resonance NMR spectroscopy.

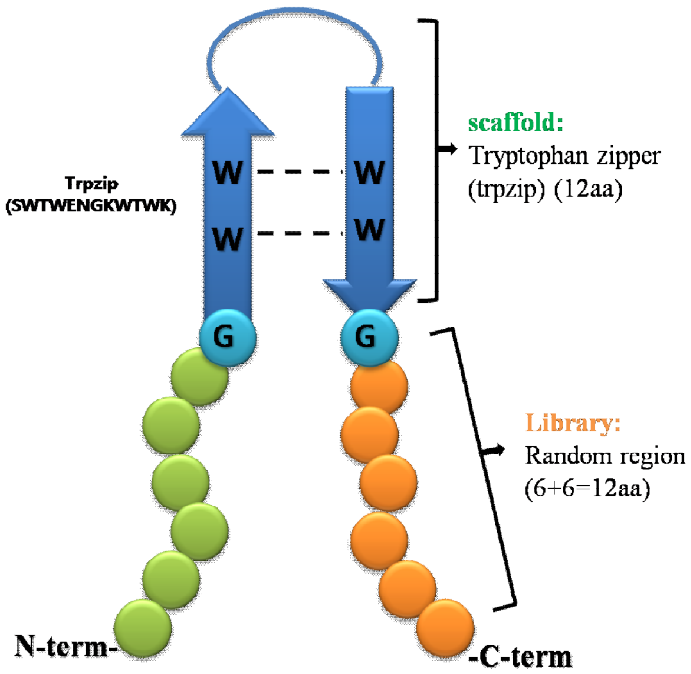

Figure 3. Structure of aptide.

The aptide has a trpzip (blue) region with tryptophan–tryptophan (W—W) cross-strand pairs as a scaffold and two randomized ligand-binding regions (green and orange) that are capable of synergistically binding the target. Each green and orange circle in the aptide represents a randomized amino acid, while the blue circles denote the glycine linkers connecting the scaffold to the randomized binding site. In this study aptide is the EDB specific binder.

1.3. Principle of NMR backbone assignment

Nuclear magnetic resonance (NMR) protein studies rely on the accurate assignment of resonances. There are four steps in the assignment process, the first of which is to pick cross peaks from the NMR experiment. Peak picking has been well automated by modern software. The second step is to group peaks from different experiments into spin systems, which is also known as clustering. This is typically done by inspecting the HN and N resonances of peaks from an 2D HSQC or multiple 3D experiments such as CBCA(CO)NH and HNCACB and grouping the peaks within certain proximity into individual clusters. The third step is to assign the clustered spin systems with residue names and residue numbers in the sequence of the protein. This is done by assessing connectivities from scalar coupled experiments and evaluating possible amino acid types. The final step in the procedure is the verification of the assignment which should be consistent between all the measured spectra (Kirby NI *et al.*, 2004).

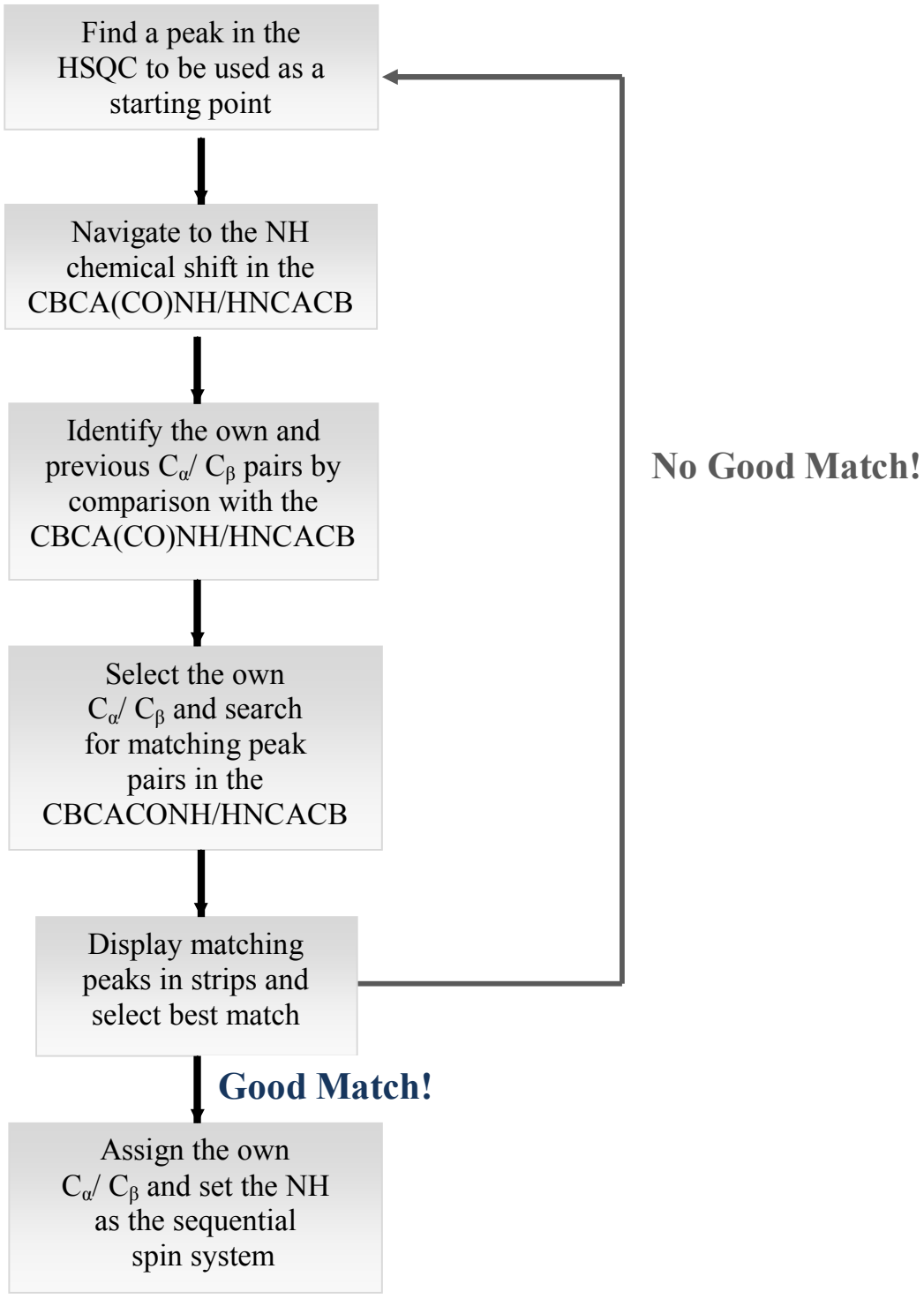

Figure 4. The flow chart diagram of Cα/ Cβ assignment process

For the assignment, 2D ^{1}H–^{15}N-HSQC, 3D-HNCACB, CBCA(CO)NH and HBHA(CO)NH spectra are recorded for NMR peak picking and analysis. 2D HSQC mainly shows the backbone amide groups, and also the Nε-Hε side-chain groups of the tryptophan residues and the Nδ-Hδ or Nε-Nε side chain groups of asparagine or glutamine residues. The HSQC spectrum is like a fingerprint of the protein and is usually the first measured heteronuclear experiment on proteins.

The triple resonance spectra for the backbone assignment have ^{1}H, ^{15}N and ^{13}C dimensions to record the individual chemical shifts. 3D experiments are generally based upon 2D experiments and so the easiest way to think of the 3D is that 2D data are arrayed and extended into the third dimension. The first two dimensions are ^{1}H and ^{15}N frequencies, respectively. This is now extended into the third dimension which is the ^{13}C dimension. So the HSQC peaks in one plane are separated into the third dimension along the ^{13}C chemical shift values that are coupled with the NH group. It is possible to inspect the 3D spectrum on various different planes and a subset of backbone shifts are observed on each plane. The ^{1}H chemical shifts are generally set for the x-axis, the ^{13}C chemical shifts for the y-axes, and the ^{15}N chemical shifts for the z-axis.

3D CBCA(CO)NH first labels $^{13}C\alpha$ and $^{13}C\beta$ frequencies and then transfer the $^{13}C\beta$ and $^{13}C\alpha$ magnetization to the preceding backbone ^{15}Nnucleus via ^{13}CO, then finally to $^{1}H^{N}$ for detection. The chemical shifts evolve simultaneously on $^{13}C\alpha$, and $^{13}C\beta$, so these appear in the same dimension. The chemical shifts ^{15}N and $^{1}H^{N}$ are separately labeled in the orthogonal axes. The chemical shift of ^{13}CO is not labeled in this

particular experiment. In the HNCACB experiment, magnetization is transferred from $^{1}H\alpha$ and $^{1}H\beta$ to $^{13}C\alpha$ and $^{13}C\beta$, respectively, and the chemical shifts of $^{13}C\beta$ to $^{13}C\alpha$ are labeled. Subsequently, the magnetization is transferred to backbone amide ^{15}N of its own and preceding residues by $^{1}J_{NC}$ and $^{2}J_{NC}$couplings, where the former is larger than the latter. After recording the chemical shifts of both ^{15}N nuclei, the magnetization finally transfers to the backbone amide $^{1}H^{N}$ for detection. Transfer from $C\alpha_{i}$ both to $^{15}N_{i}$ and $^{15}N_{i-1}$ results in two sets of spin systems, in which the cross peak intensities originating from the intra-residue spin system are in most cases larger than those from the inter-residue spin systems. Thus, for each backbone NH group, there are strong Cα and Cβ cross peaks and weaker ones. The chemical shifts evolve simultaneously on $^{13}C\alpha$ and $^{13}C\beta$, so they appear in the same dimension (Fig. 5). The chemical shifts of ^{15}N and $^{1}H^{N}$are labeled separately in orthogonal axes, as is observed in the CBCA(CO)NH experiment.

Another 3D experiment is HBHA(CO)NH. magnetization is transferred from$^{1}H\alpha$ and $^{1}H\beta$ to $^{13}C\alpha$ and $^{13}C\beta$, respectively, and then from $^{13}C\beta$ to $^{13}C\alpha$. From here it is transferred first to^{13}CO, then to $^{15}N^{H}$ and then to $^{1}H^{N}$ for detection. The chemical shift it not evolved on any of the carbon atoms. Instead, it is evolved on the $^{1}H\alpha$ and$^{1}H\beta$, the $^{15}N^{H}$ and $^{1}H^{N}$. This results in a three-dimensional spectrum with one nitrogen and two hydrogen dimensions (Fig. 5).

Together with the CBCA(CO)NH and HSQC, HNCACB forms the standard suite of triple resonance experiments needed for the backbone assignment. For large proteins the signal-to-noise may not be great and other triple resonance experiments

such as HNCA, HN(CO)CA, HNCO and HN(CA)CO can be useful to assist and confirm the assignment (Table. 1). (Higman VA *et al.*, 2012).

1.4. Chemical Shift Index

A simple technique for identifying protein secondary structures employs the analysis of backbone ^{13}C chemical shifts. It is called the Chemical Shift Index (Wishart D S *et al.*,1991) which was originally developed for the analysis of $^{1}H_{\alpha}$ chemical shifts. By extending the Chemical Shift Index to include $^{13}C\alpha$, $^{13}C\beta$ and carbonyl ^{13}C chemical shifts, it is now possible to use four independent chemical shift measurements to identify and locate protein secondary structures based on chemical shift differences with respect to some predefined 'random coil' values.

It can be applied from the measured Hα, Cα, Cβ and CO chemical shifts for each residue in a protein. The Cα, Cβ and CO chemical shifts relative to random coil shifts have a clear correlation with the polypeptide torsion backbone angles φ and ψ. For example, for the Cβ resonance a downfield shift from the random coil position is observed for extended β-sheet structure, with ψ ~130°, whereas for α-helical structures a small upfield shift is observed (ψ ~−50°).

Based on these observations, the local secondary structure can be predicted using the Cα, Cβ and CO chemical shifts by either plotting the secondary shifts (= observed shift – random coil shift) or by using the chemical shift index (CSI) program (Wishart

D S *et al*., 1994), which gives a consensus value using all of the secondary shifts from the Cα, Cβ and CO nuclei and has an output of +1 for beta-strand, 0 for random coil and -1 for α-helix. Thus, the secondary structure of peptides and proteins can be accurately predicted from ^{1}H and ^{13}C chemical shifts, without recourse to the NOE measurements. (Wishart D S *et al.*, 1992).

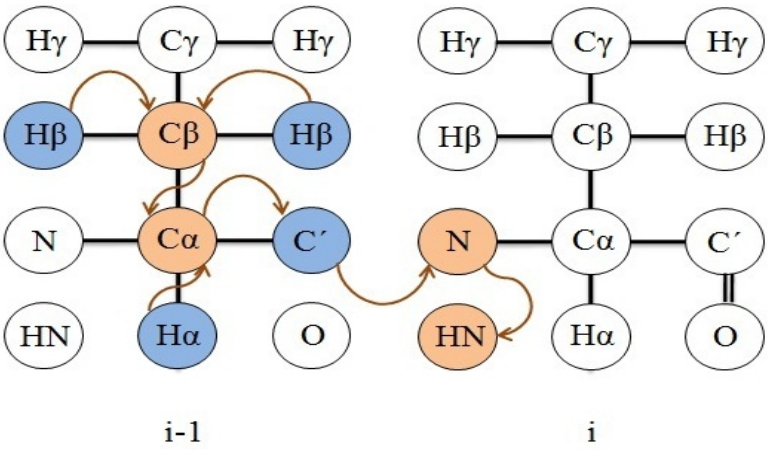

CBCA(CO)NH

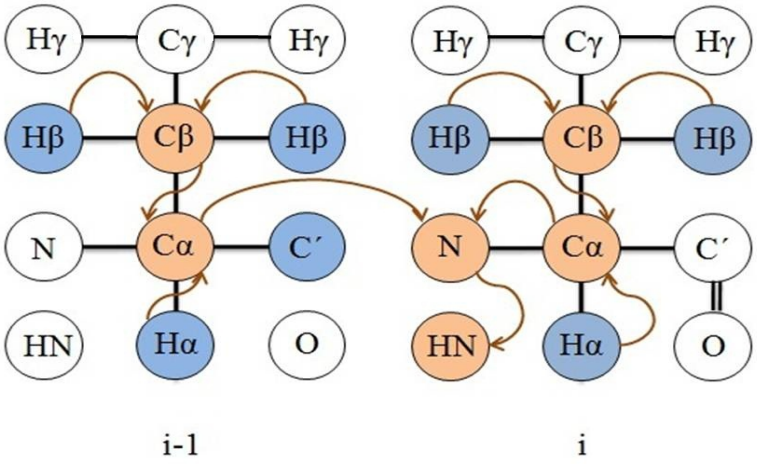

HNCACB

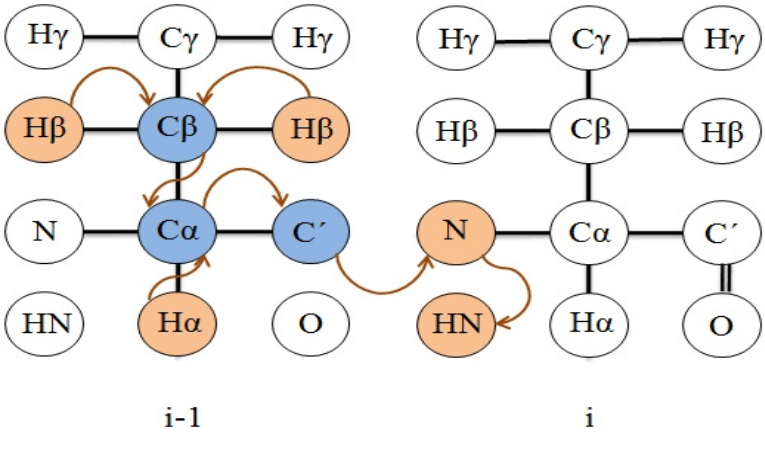

HBHA(CO)NH

Figure 5. The magnetization transfer in HNCACB, CBCA(CO)NH and HBHA(CO)NH

Table 1. Nuclei correlated in 3D NMR experiment

Experiment	$C\beta_{(i-1)}$	$C\alpha_{(i-1)}$	$CO_{(i-1)}$	H^N	N^H	$C\alpha$	$C\beta$	$H\alpha$	$H\beta$
HNCO			■	■	■				
HNCA		■		■	■	■			
HN(CO)CA		■		■	■				
CBCA(CO)NH	■	■		■	■				
HNCACB	■	■		■	■	■	■		
HBHA(CO)NH				■	■			■	■

II. MATERIALS AND METHODS

2.1 . Protein expression and purification

Bacterial strains and plasmids

Escherichia coli DH5α and BL21(DE3)were used for DNA manipulation and protein overexpression. EDB and aptide protein coding sequences were PCR amplified using DNA *pfu*Tag polymerase (Stratagene) and modified pET-32a as the template. The PCR products were digested by NcoI (Thermo Fisher Scientific) and XhoI (Thermo Fisher Scientific) restriction enzyme and sub-cloned into the modified pET-32a vector with N-terminal His_6 / Trx tag separated by a thrombin cleavage site.

EDB amino acid sequence

EVPQLT DLSFVDITDS SIGLRWTPLN SSTIIGYRIT VVAAGEGIPI

FEDFVDSSVG YYTVTGLEPG IDYDISVITL INGGESAPTT LTQQT

Aptide amino acid sequence

SSSPIQGSW TWENGKWTWK GIIRLEQ

Figure 6. Amino acid sequence of EDB and aptide

Table 2. The composition of medium

Medium	Composition (/ L)
LB medium	1 % tryptone, 0.5 % yeast extract, and 1 % NaCl
M9 minimal medium (^{15}Nitrogen)	10 g K_2HPO_4, 13 g KH_2PO_4, 9 g Na_2HPO_4, 2.4 g K_2PO_4, 1.0g $^{15}NH_4Cl$, 5 g Glucose, 10 mM $MgCl_2$, 0.1 mM Thiamine, 1 x trace elements, 0.2 mM $CaCl_2$, 50 ug/ml carbenicillin.
M9 minimal medium (^{13}Carbon, ^{15}Nitrogen)	10 g K_2HPO_4, 13 g KH_2PO_4, 9 g Na_2HPO_4, 2.4 g K_2PO_4, 1.0 g $^{15}NH_4Cl$, 2.0 g U-^{13}C6 Glucose, 10 mM $MgCl_2$, 0.1 mM Thiamine, 1 x trace elements, 0.2 mM $CaCl_2$, 50 ug/ml carbenicillin.
M9 minimal medium for 1L D_2O (99.9 %) (^{2}H, ^{13}Carbon, ^{15}Nitrogen)	10 g K_2HPO_4, 13 g KH_2PO_4, 9 g Na_2HPO_4, 2.4 g K_2PO_4, 1.0 g $^{15}NH_4Cl$, 2.0 g U-^{12}C-U-^{2}H-D-Glucose, 0.2 mM $CaCl_2$, 952 mg $MgCl_2$, 34 mg Thiamine, lyophilize 10 ml of trace elements (Dissolve in D_2O), 100 mg carbenicillin, 1 g $^{2}H/^{13}C/^{15}N$ of IsoGro

Protein expression and purification

EDB and aptide plasmids were introduced into *Escherichia coli* strain BL21(DE3), respectively, and the transformation was grown in either Luria Bertini (BD, 244620) or minimal medium at 37℃ (Table. 2). The cells transformed by expression vector were cultured at 37℃ to an OD_{600} of ~0.8. For overexpression of EDB and aptide protein, the cell were induced by 1mM Isopropyl β-D-1-thiogalactopyranoside (IPTG, Gold biotechnology, 12381C25), and allowed to express for 4-6 hours.

The cell were harvested by centrifugation, For purification of EDB (Fig. 7), the cell pellet was resuspended with 50 ml (per liter of culture) of 20 mM Tris-HCl (pH 7.4), 200 mM NaCl and 1 mM Phenylmethylsulfonyl fluoride (PMSF, Sigma, P7626). The suspension was lysed by Emulsiflex after homogenizing, and centrifuged at 24000 Xg (Beckman JLA-16.250) for 20 min at 4℃. The supernatant fraction was loaded onto Ni^{2+}-NTA column (GE Healthcare, 17-5255-01) and the protein was eluted with a 20 mM Tris-HCl (pH 7.4), 200 mM NaCl and 500 mM imidazole after washing with a 20 mM Tris-HCl (pH 7.4), 200 mM NaCl. The eluted protein was exchanged to 20 mM Tris-HCl pH 7.4, 200 mM NaCl, and digested with thrombin (sigma, S6684) for 12 hours at room temperature followed by inactivation of thrombin via addition of 5 mM benzamidine (Sigma, 434760).

The cleaved His_6 - thioredoxin (sigma, S6684) was removed by loading the digested proteins over a Ni^{2+}-NTA column and eluted with 20mM Tris-HCl (pH 7.4), 200 mM NaCl (Fig 7). And then, EDB was concentrated by Amicon ultra centrifugal filter

(Millipore, UFC901096). After buffer exchange, EDB was purified by superdex-75 gel filtration (GE Healthcare, 17-1070-01).

For purification of aptide (Fig. 8) inserted in pET-32a vector, the cell pellet was resuspended with 50 ml (per liter of culture) of 20 mM Tris-HCl (pH7.4), 1 mM Phenylmethylsulfonyl fluoride. The suspension was lysed by Emulsiflex after homogenizing, and centrifuged at 24000 Xg (Beckman JLA-16.250) for 20 min at 4℃.

The supernatant fraction was loaded onto a Ni^{2+}-NTA column (GE Healthcare) and the protein was eluted with a gradient of buffer composed of 20 mM Tris-HCl (pH 7.4) and 500 mM imidazole. The eluted protein was exchanged to 20 mM Tris-HCl (pH 7.4), 200 mM NaCl, and digested with thrombin for 12 hours at room temperature followed by inactivation of thrombin via addition of 5 mM benzamidine.

The cleaved His_6 - thioredoxin was removed by loading the digested proteins over a Ni^{2+}-NTA column and eluted with eluted with a gradient of buffer composed of 20 mM Tris-HCl (pH 7.4) and 500 mM imidazole. The eluted fractions containing EDB and aptide were analyzed by SDS-PAGE to confirm the sample mass and sample purity.

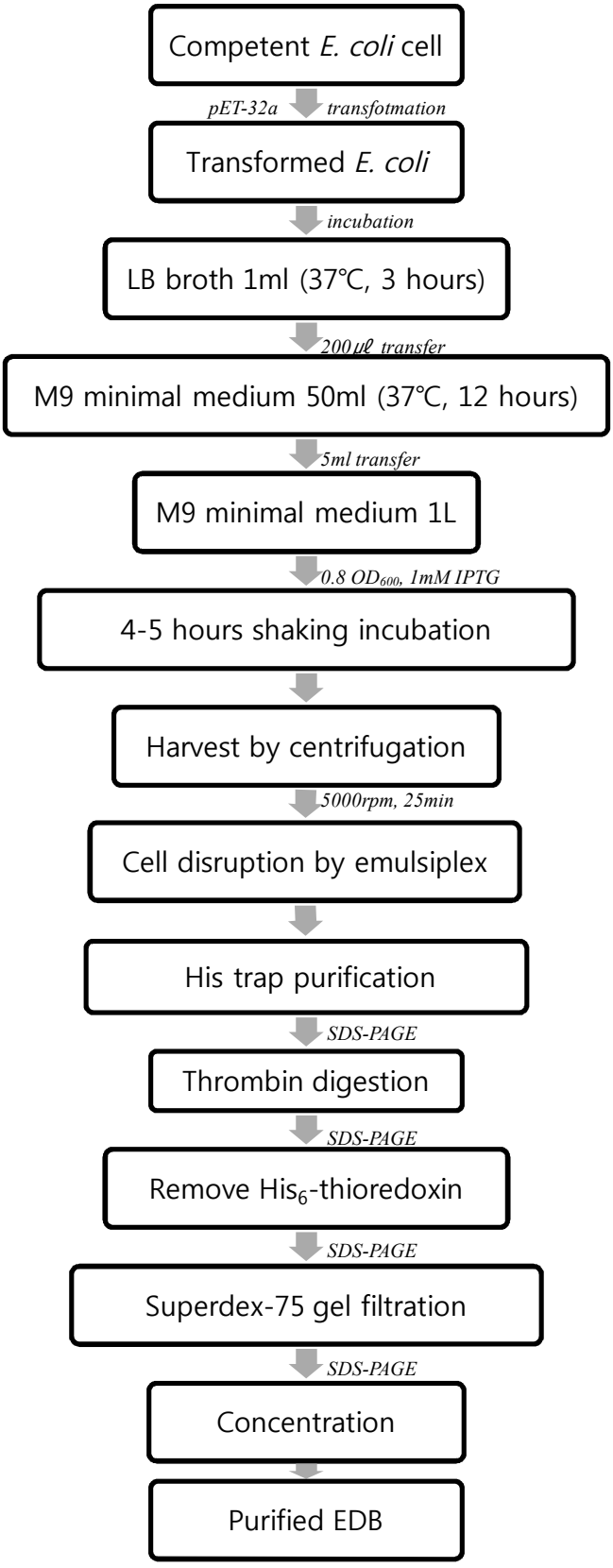

Figure 7. Purification procedure of recombinant EDB

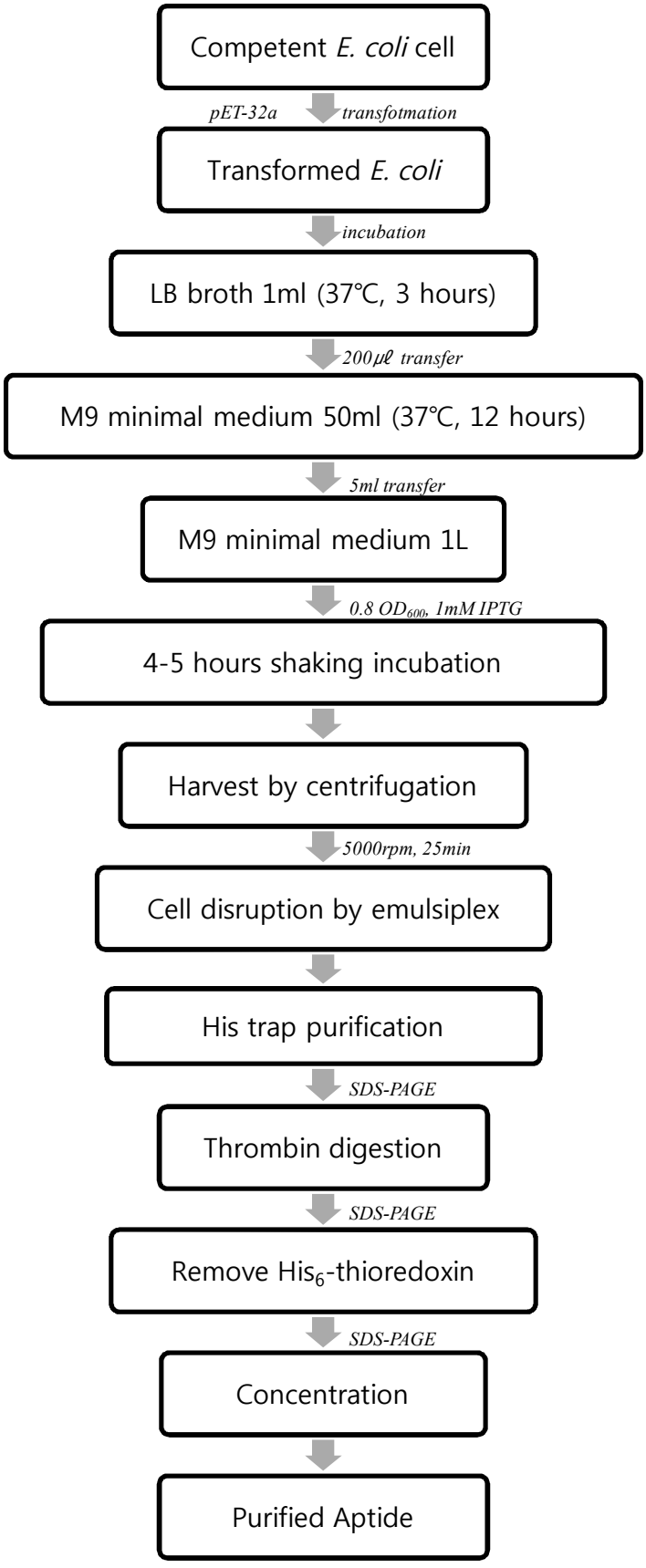

Figure 8. Purification procedure of recombinant Aptide

Sample preparation and isotope labeling

[$^{13}C/^{15}N$], [$^{2}H/^{13}C/^{15}N$] - labeled proteins have been most useful for increasing the sensitivity of triple resonance NMR experiments commonly used for backbone assignments of proteins. The uniformly [^{15}N], [$^{15}N/^{13}C$] and [$^{2}H/^{13}C/^{15}N$] labeled proteins were prepared from *E. coli* strain BL21(DE3). M9 minimal medium, which contained $^{15}NH_4Cl_2$. ^{13}C-glucose was used for the growth of the cell.

The overexpressed EDB and aptide protein were eluted by His-Tag affinity column. Then a N-terminal oligohistidine was digested by thrombin protease and re-eluted by His-Tag affinity column. The final purification step was the gel filtration column. The eluted protein solution was concentrated. The concentration of NMR sample was approximately 0.3mM for [$^{13}C/^{15}N$] - labeled EDB protein and aptide.

2.2. NMR experiments

The triple [$^{2}H/^{15}N/^{13}C$] labeled EDB and EDB:aptide complex protein solution were used as a sample for 2D HSQC and triple resonance experiments. NMR experiments were acquired on a Bruker 600, 800, 900 MHz (Seoul National University and Korea Basic Science Institute) z-shielded gradient triple resonance cryoprobe at 298K.

EDB free and EDB:aptide complex protein dissolved in 20mM sodium phosphate buffer containing 0.01 % sodium azide and 10 % D_2O. The double [^{13}C, ^{15}N] labeled / triple [^{1}H, ^{13}C, ^{15}N] labeled complex solution were used as a sample for three triple resonance spectra: HNCACB (Wittekind M *et al*., 1993), CBCA(CO)NH (Grzesiek S *et al*., 1993) and HBHACONH (Grzesiek S *et al*., 1993) were collected at pH 6.0. Table. 3 and 4 show NMR experiments parameter of EDB free form and EDB with aptide complex.

Table 3. NMR experiments parameter of EDB free form

3D- CBCA(CO)NH

Index	MHz	axis	width (Hz)	center	points
HN	800.254	x	8802.817	4.774	512
^{15}N	81.098	y	2270.663	118.082	32
^{13}C	201.231	z	14104.372	40.745	64

3D-HNCACB

Index	MHz	axis	width (Hz)	center	points
HN	800.254	x	8802.817	4.772	512
^{15}N	81.098	y	2270.663	118.081	32
^{13}C	201.231	z	14104.372	40.744	64

2D-HSQC

Index	MHz	axis	width (Hz)	center	points
HN	800.254	x	8802.817	4.769	512
^{15}N	81.098	y	14084.507	40.741	98

Table 4. NMR experiments parameter of EDB:aptide complex

3D-CBCA(CO)NH

Index	MHz	axis	width (Hz)	center	points
HN	900.23	x	10822.511	4.773	512
^{15}N	91.230	y	2737.476	118.082	28
^{13}C	226.372	z	14947.683	42.737	48

3D-HNCACB

Index	MHz	axis	width (Hz)	center	points
HN	900.23	x	10822.511	4.773	512
^{15}N	91.230	y	2737.476	118.082	28
^{13}C	226.372	z	14947.683	42.737	60

3D-HBHA(CO)NH

Index	MHz	axis	width (Hz)	center	points
HN	800.254	x	9615.385	4.771	512
^{15}N	81.098	y	2433.090	118.074	25
^{1}H	800.254	z	4800.768	3.271	64

2D-HSQC

Index	MHz	axis	width (Hz)	center	points
HN	900.23	x	12626.263	4.773	512
^{15}N	91.230	y	2919.366	118.082	98

NMR data processing and analysis

Three-dimensional data sets were processed on a Silicon Graphics Indy workstation using a combinational of software written at National Institutes of Health (nmrPipe, nmrDraw). The programs PIPP (Garrett D S *et al*., 1991) was used for peak picking and spectra analysis. Two-dimensional data sets were processed using nmrPipe and nmrDraw (Delaglio S *et al,* 1995).

Ⅲ. Results and Discussion

3.1. sample preparation of EDB and aptide

EDB is a protein with 91 amino acids and the molecular weight of 10 KDa. The vector system for EDB was pET-32a, which contains Novagen His-Tag with six histidines. These additional hexa-his tag made the purification of protein easier and reliable. Unlabeled LB media sample and uniformly [^{15}N], [^{13}C, ^{15}N], [^{2}H, ^{13}C, ^{15}N] labeled EDB are prepared from the overproducing *E. coli* strain BL21(DE3) containing the plasmid EDB in pET-32a vector. The T7 RNA polymerase system including pET-32a vector is widely used for the recombinant protein expression. Since the T7 RNA polymerase elongates chains about five times faster than the *E. coli* RNA polymerase, the proteins from genes preceded by the T7 promoter are expressed at higher levels.

Therefore, I used a plasmid containing the T7 promoter to express EDB. EDB construct was successfully cloned and could be highly expressed in *E. coli* BL21(DE3). Recombinant protein in the supernatant was purified by two chromatography steps; His–Bind Ni^{2+}-NTA column and gel filtration superdex 75 column. The result was sufficient for NMR measurement (Fig 9). The final concentration of EDB was about 2.0mM.

Aptide is a peptide with 25 amino acids and the molecular weight of 3.1 KDa. The vector system for aptide was pET-32a, which contains Novagen His-Tag with six histidines. Unlabeled LB media sample was prepared from the overproducing *E. coli*

strain BL21(DE3) containing the plasmid aptide in pET-32a vector. Aptide construct was successfully cloned and could be highly expressed in *E. coli* BL21(DE3). Recombinant protein in the supernatant was purified by one chromatography step; His–Bind Ni^{2+}-NTA column. The result was sufficient for NMR measurements (Fig. 10). The final concentration of aptide was about 1.5mM.

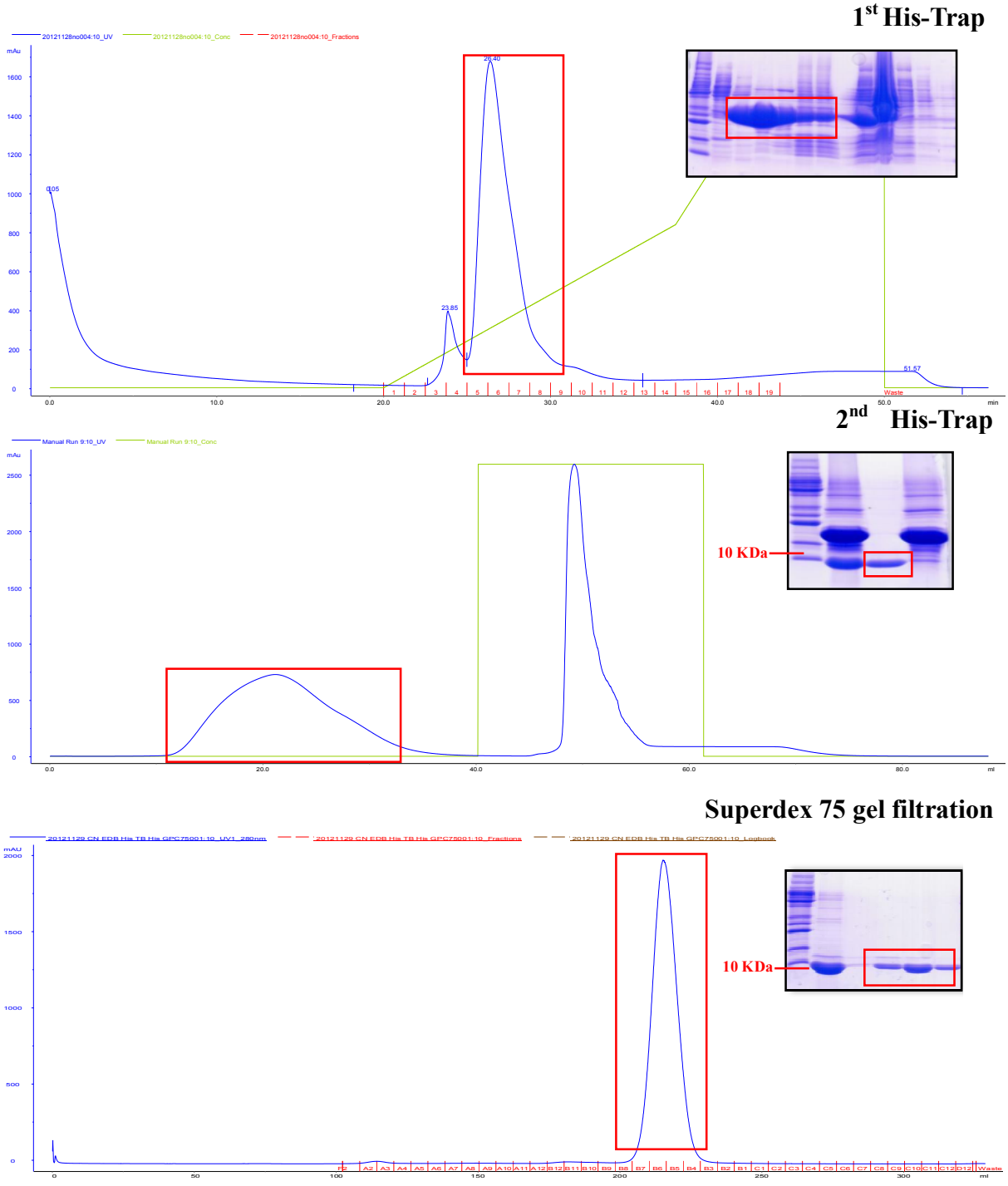

Figure 9. Purification of EDB

The overexpressed EDB protein was eluted by His-Tag affinity column. Then a N-terminal oligohistidine was digested by thrombin protease and re-eluted by His-Tag affinity column. The final purification step was the gel filtration column.

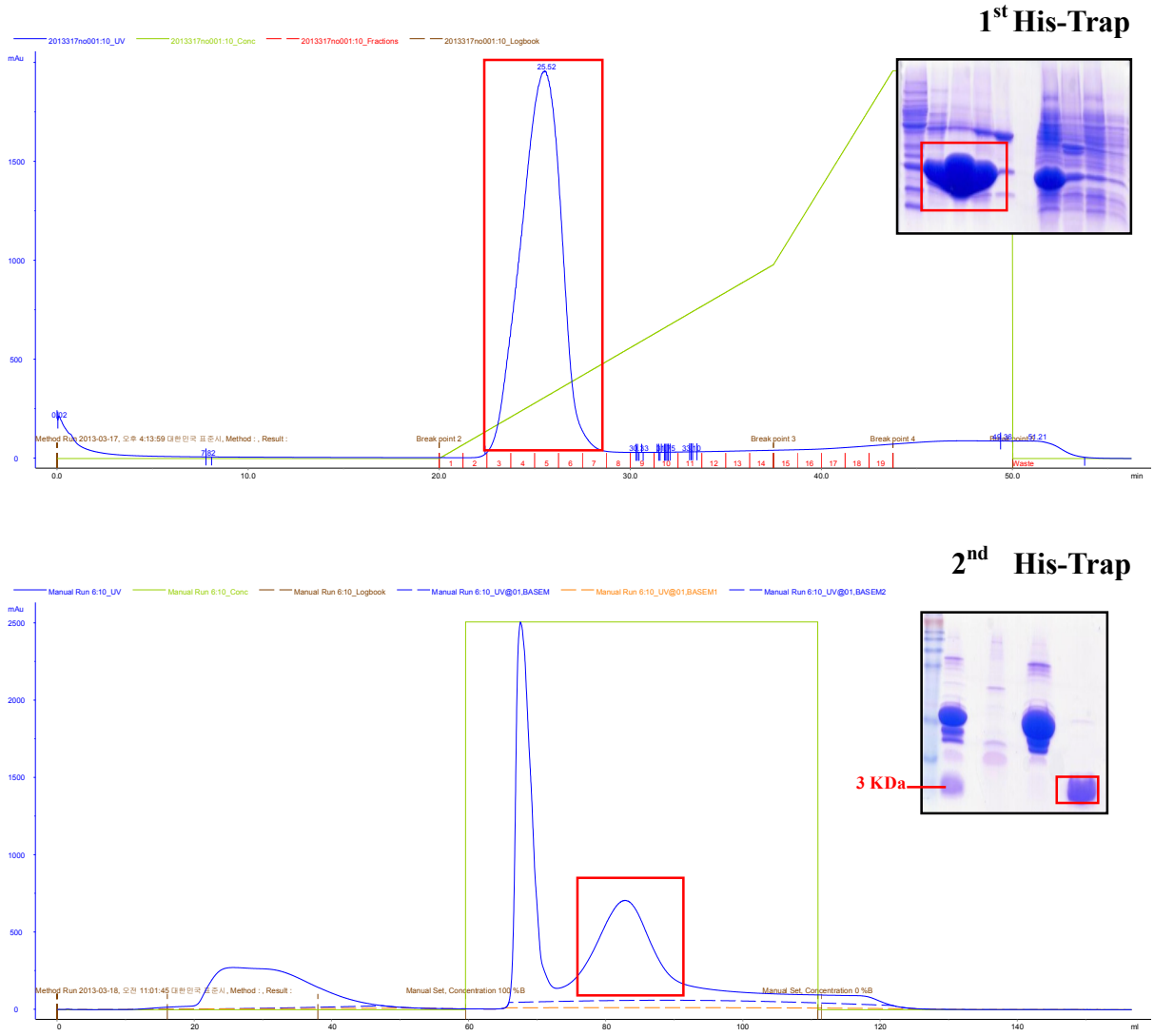

Figure 10. Purification of aptide

The overexpressed aptide protein was eluted by His-Tag affinity column. Then a N-terminal oligohistidine was digested by thrombin protease and re-eluted by His-Tag affinity column.

3.2 NMR assignment

Backbone chemical shift assignment

In order to determine the high-resolution structure of EDB-aptide complex, I employed the solution NMR spectroscopy. The resonances in the HSQC spectra show EDB in the free state (black) and in the EDB:aptide complex (red) (Fig. 11). I could observe large chemical shift changes of backbone amide groups of EDB upon complex formation with aptide. The NMR titration between EDB and aptide indicated a slow exchange on the chemical shift time scale. To identify the cross peaks in the 2D HSQC spectra in the free and complex state, set on backbone assignment using the conventional sequential assignment strategy. First obtained 3D-CBCA(CO)NH, HNCACB and HBHA(CO)NH spectra for assignment on 900 MHz and 800 MHz Bruker Avance II spectrometer. I performed peak picking and clustering to identify the spin systems using the software PIPP.

Sequential assignment was achieved by verifying and linking of peak clusters obtained from the triple NMR experiments. The peaks in the nearest neighborhood could be combined into a new peak cluster, when the H^N and ^{15}N chemical shifts represent a unique spin system. The cluster from 2D HSQC experiment combines the inter-residue ^{13}C chemical shifts from CBCA(CO)N H, and then the intra-residue ^{13}C chemical shifts, so that each spin system harbors the intra- and inter- residue chemical shifts ($^{15}N_i$, H^N_i, $^{13}C\alpha_i$, $^{13}C\beta_i$, $^{13}C\alpha_{i-1}$ and $^{13}C\beta_{i-1}$).

For example, Fig. 12 shows a peak cluster composed of 7 peaks originating from a Val77 residue. Based on the chemical shift statistics in the BioMagResBank (http://www.bmrs.wisc.edu), the program suggests possible amino acid candidates for each cluster. These clusters could be sequentially linked according to $^{13}C\alpha$, $^{13}C\beta$ chemical shifts of the cluster and the protein sequence. Fig. 13 shows a series of strip plots selected from the 3D CBCA(CO)NH and HNCACB spectra of EDB.

The insets show cross-sections that were taken parallel to the ^{1}H axis at the position, indicated by the horizontal broken lines. The strips were taken at the ^{15}N chemical shifts (indicated at the bottom of the strips) of amino acid residues Leu29, Asn30, Ser31, Ser32, and Thr33, where the amide proton chemical shifts appear in the center of each plot. Fig. 13a–13e strip plots were taken from the CBCA(CO)NH spectrum, which shows exclusively $^{13}C\alpha$,$^{13}C\beta$ inter-residue ($i - 1$) correlations. Fig. 13 a'–e' strip plots were taken from the HNCACB spectrum, which shows both intra-residue (i) and inter-residue ($i - 1$) correlations. Horizontal and vertical lines denote the ^{13}C and $^{1}H^{N}$ chemical shifts that have connectivities from the 3D spectra described above. With these connectivities, nearly complete resonance assignment of backbone $^{1}H^{N}$, ^{15}N, $^{13}C\alpha$, and $^{13}C\beta$ nuclei could be achieved for this protein.

Figure 14 shows the strip plots from the 3D correlation spectra of EDB:aptide complex showing connectivities for the region Val15, Asp16, Ile17, Thr18, and Asp19. Figure 15 shows the HBHA(CO)NH of the Val15 and Asp16 residue preceding the observed amide in the HSQC spectrum of EDB:aptide complex. The x-axes of the individual spectrum represent the $^{1}H^{N}$ chemical shifts and the y-axes of the individual

spectrum represent the ^{1}Hα chemical shifts of the same $^{1}H^{N}/^{15}$N-edited slice. Each peak at the center of the crosshair belongs the same ^{1}H and ^{15}N chemical shifts. In this manner, I could obtain the Hα chemical shifts through HBHA(CO)NH spectra. In summary, a total of 80 % of the ^{13}Cα and ^{13}Cβ resonances of free EDB has also assigned (Table. 5), and a total of 97 % of the ^{1}Hα, 97 % of the ^{13}Cα and 97 % of the ^{13}Cβ resonances of EDB:aptide complex has also assigned (Table. 6).

The missing assignments correspond to proline residues or residues adjacent to prolines. In case of EDB in the free state, a set of ^{1}H and ^{15}Nassignmentis available in the BMRB for comparison, and also the three-dimensional structure in the free state is available with the PDB ID 2FNB (Wuthrich et al., 1998). Figure 16 and 17 show 2D ^{1}H-^{15}N HSQC spectrum of EDB free form and EDB:aptide complex annotated with the assignment in the current study.

Lastly, Figure 18 shows chemical shift mapping of aptide binding to the EDB.

CSI of EDB and EDB:aptide complex

The chemical shift index plot for Hα, Cα, and Cβ of EDB and EDB:aptide complex are shown in Figure 19, 20, 21 and 22. There is a good correlation in the type of secondary structure between among the CSI values. In free EDB, most residues have a positive index in the Hα plot, indicating the predominant β-strand secondary structures. In the Cα plot, most residues have negative CSI values (Fig. 19). In the Cβ plot most residues have positive CSI values. The consensus (^{1}Hα, ^{13}Cα, and ^{13}Cβ chemical shifts when available) chemical shift index results indicate that seven β-strand secondary structures are found in residues 9-15, 20-26, 33-42, 51-55, 61-65, 74-81, and 90-94 (Fig. 20). In EDB:aptide complex, most residues have a positive index in the Hα plot as expect for β-strand secondary structure. In the Cα plot, most residues have a negative index (Fig. 21). And in Cβ plot, most residues have a positive index. The consensus (^{1}Hα, ^{13}Cα, and a subset of ^{13}Cβ chemical shifts) chemical shift index results indicate that six β-strand secondary structure is found in the region of residues 5-15, 20-28, 34-42, 51-55, 62-64 and 72-80 and a α-helix turn appeared in the region of residues 56-59 (Fig. 22).

Compared to the CSI of free EDB, CSI data of EDB:aptide complex show a large change in the secondary structure upon binding (Fig. 23). Our results suggest that the interaction between EDB and aptide likely involves a large conformational change in EDB. A detailed description of the conformational change awaits the complete side-chain assignments, NOE measurement, and the structure calculation.

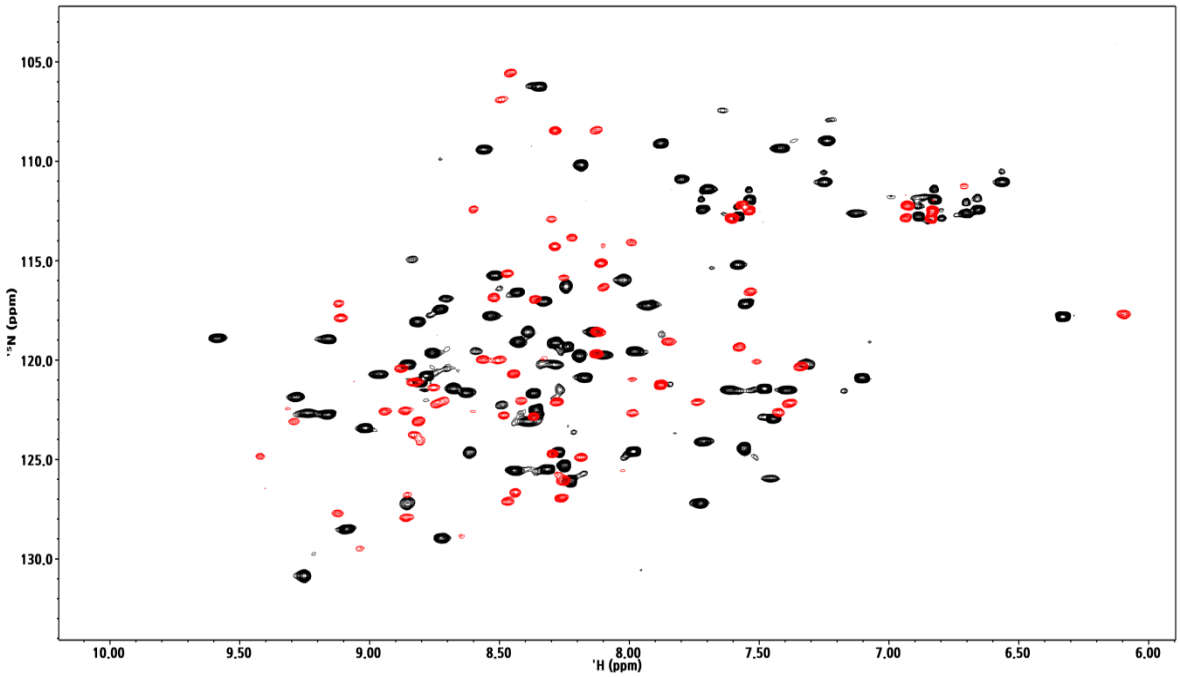

Figure 11. ^{1}H-^{15}N HSQC spectrum of uniformly ^{15}N-labeled EDB in the free state and in complex with aptide

in sodium phosphate buffer, pH 6.0. The spectrum was measured at 25℃ and sample concentration was 0.3mM. This figure was made using the NMRViewJ program.

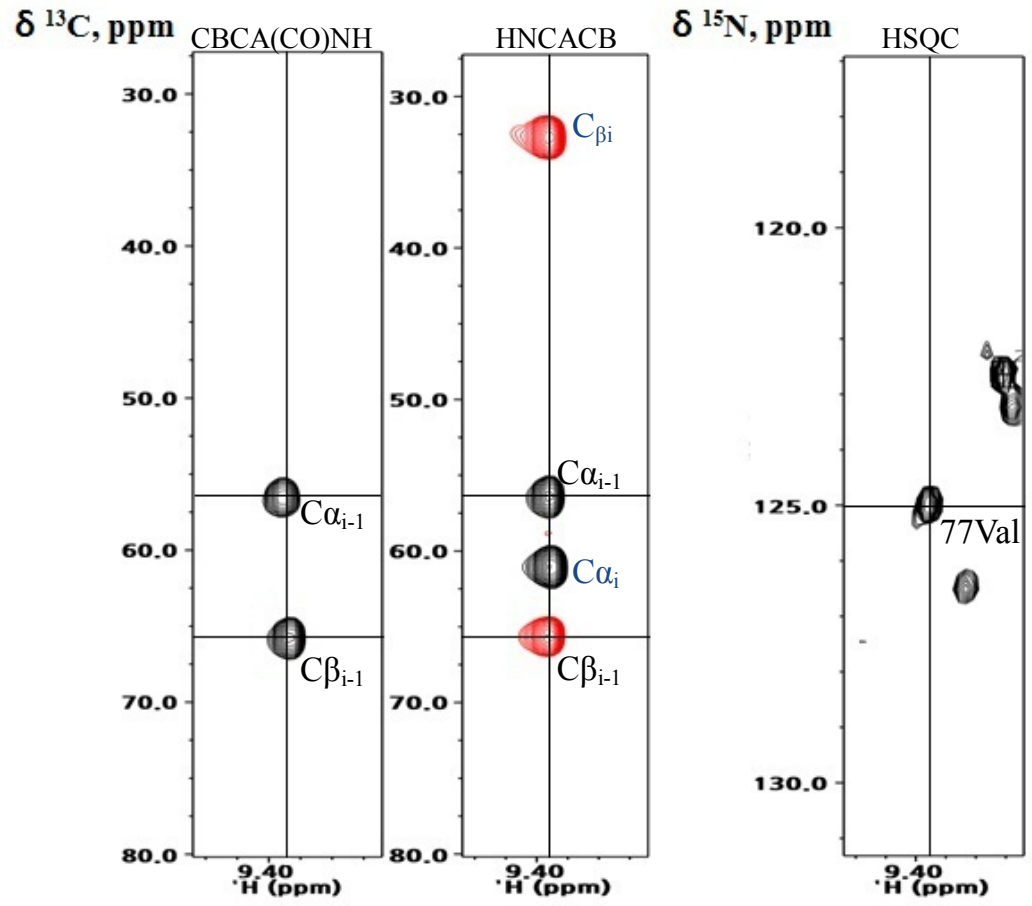

Figure 12. Verification of peak clusters for the spin system identification.

The 7 peaks are combined into a peak cluster. The x-axes of the individual spectrum represent the H^N chemical shifts and the y-axes of the individual spectrum represent the ^{13}C labeled carbon chemical shifts of the same ^{15}N-edited slice. Each peak at the center of the crosshair in each spectrum appears with the same ^{1}H and ^{15}N chemical shifts. This figure was made using the NMRViewJ program.

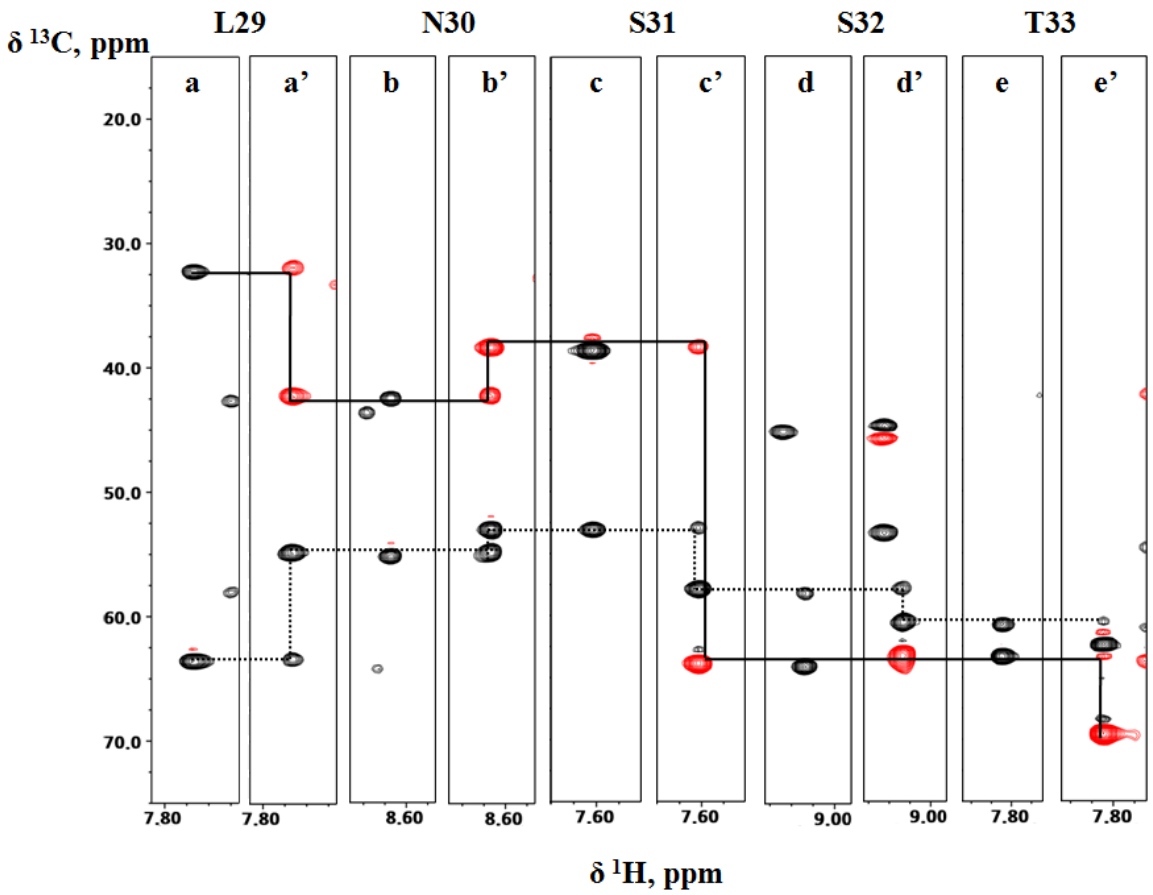

Figure 13. Strips of selected from a 3D HNCACB and CBCA(CO)NH spectra of EDB (free). In this figure, the strips containing HNCACB and CBCA(CO)NH resonances of residues of 15-19 are shown for Cα (dashed line) and Cβ (solid line). a', b'. c', d' and e' are HNCACB strips, a, b, c, d and e are their corresponding CBCA(CO)NH strips. This figure was made using the NMRViewJ program.

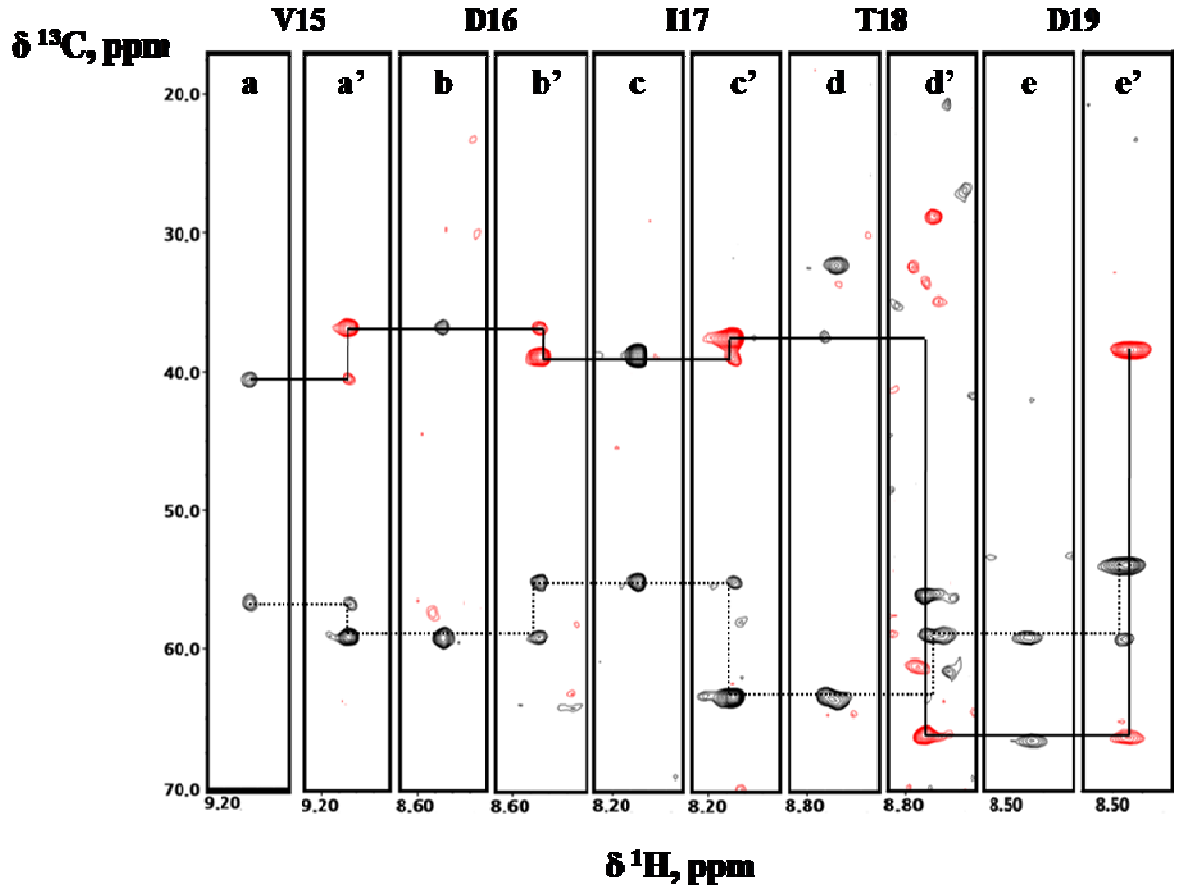

Figure 14. The strip plot of HNCACB and CBCA(CO)NH spectra between residues15–19of EDB in the EDB:aptide complex

In this figure, the strips containing HNCACB and CBCA(CO)NH resonances of residues of 15-19 are shown for Cα (dashed line) and Cβ (solid line). a', b'. c', d' and e' are HNCACB strips, a, b, c, d and e are their corresponding CBCA(CO)NH strips. This figure was made using the NMRViewJ program.

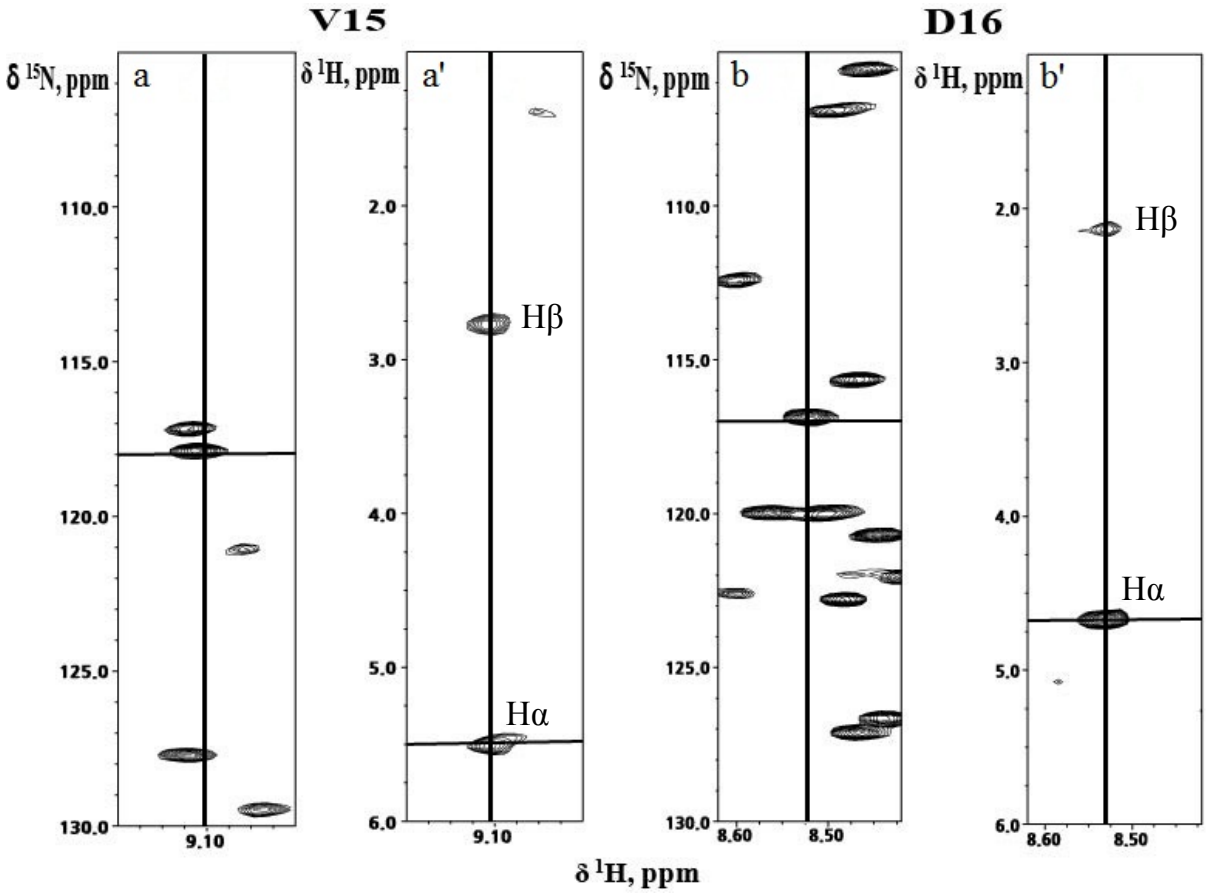

Figure 15. The strip plot of HBHA(CO)NH for residues Val15 and Asp16 of EDB in the EDB:aptide complex

The x-axes of the individual spectrum represent the H^N chemical shifts and the y-axes of the individual spectrum represent the ^2H labeled proton α chemical shifts of the same $^1H/^{15}N$-edited slice. Each peak at the center of the crosshair in each spectrum appears with the same ^1H and ^{15}N chemical shifts. a' and b' are HSQC strips, a and b are their corresponding HBHA(CO)NH strips. This figure was made using the NMRViewJ program.

Table 5. Chemical shift for ^{1}H, ^{13}C, and ^{15}N backbone resonances for free EDB

Residue	^{1}H	^{15}N	$^{13}C\alpha$	$^{13}C\beta$
S4	8.69	115.79	58.53	64.08
E5	8.51	122.32	55.61	32.84
V6	8.27	125.51	59.77	33.29
P7				
Q8	8.13	118.29	54.06	32.21
L9	8.21	120.69	55.63	43.55
T10	8.24	109.87	62.26	70.08
D11	7.62	121.63	52.50	40.29
L12	7.51	121.45	46.06	46.06
S13	9.32	121.76	66.48	66.48
F14	8.27	118.20	54.86	40.90
V15	9.13	118.95	60.14	35.56
D16				
I17				
T18				
D19	8.47	116.21	56.28	40.16
S20	7.90	108.88	57.27	65.86
S21	7.58	117.10	57.12	66.76
I22	8.43	118.93	61.07	43.37
G23				
L24	9.11	123.77	53.39	45.73
R25	8.81	119.66	54.36	33.83
W26	8.39	122.55	56.08	29.87
T27	9.61	118.87	60.84	68.24
P28				
L29	7.73	124.20	54.88	42.30
N30	8.63	119.71	53.01	38.40
S31	7.60	115.26	57.91	63.87
S32	9.06	123.64	60.58	63.28

T33	7.82	110.84	62.39	69.58
I34	7.13	121.13	61.67	38.09
I35	8.66	121.59	61.52	38.53
G36	7.26	109.12	44.62	38.82
Y37	8.56	115.73	56.09	41.15
R38	9.19		54.05	33.80
I39	8.79	128.93	60.04	40.72
T40	8.90	118.08	60.57	71.68
V41				
V42				
A43				
A44	8.31	125.99	56.16	59.77
G45				
E46	8.05		54.14	40.52
G47	8.28	108.52	45.37	45.37
I48	7.36	120.19	57.97	39.87
P49				
I50	8.50	121.02	56.34	29.94
F51				
E52	7.64	124.33		33.35
D53	8.82	120.70	52.30	44.55
F54	8.82	121.46	56.73	42.65
V55	8.53	118.31	58.72	35.56
D56	8.26	119.17	54.56	42.15
S57	7.72	111.40	61.00	63.72
S58	8.69	117.23	58.88	64.47
V59	7.75	127.08	64.21	32.42
G60	7.45	109.45	43.50	
Y61	6.35	117.59	55.89	41.43
Y62	8.31	124.92	58.83	43.45
T63	7.49	123.10	62.04	69.82
V64				

T65	7.93	117.10	59.99	71.19
G66	8.40	106.10	46.14	
K67	8.07	119.15	55.92	30.61
E68	8.47	122.75	55.98	29.61
P69				
G70	8.33	109.12	46.02	
I71	7.51	121.45	58.81	39.83
D72	8.17	124.27	53.17	
Y73	8.76	122.85	58.11	41.27
D74	9.19	122.57	54.05	33.80
I75				
S76	9.05	120.75	56.36	66.07
V77	8.43	120.15	61.44	33.40
I78	9.25	130.90		
T79	8.72	125.39		69.45
L80	8.51	125.67	54.35	43.65
I81	7.98	115.29		41.88
R82	8.93	120.05	54.84	37.63
G83	8.92	115.53	45.78	
G84	7.56	107.18	45.72	
E85	8.26	115.35	54.62	
S86	8.82	117.02	58.25	66.48
A87	8.25	126.85	50.59	18.23
88				
T89	7.87	119.70		
T90				
L91				
T92	8.40	116.69	61.27	70.93
Q93	9.06	125.89		
Q94	8.49	123.73	55.34	29.02
T95				

Table 6. Chemical shift for ^{1}H, ^{13}C, and ^{15}N backbone resonances for EDB-Aptide complex

Residue	^{1}H	^{15}N	Hα	$^{13}Cα$	$^{13}Cβ$
S4			4.39	58.29	63.78
E5	8.44	121.95	4.40	55.61	31.95
V6	8.26	122.17	4.06	56.38	29.50
P7					
Q8					
L9	7.77	123.82	4.49	54.82	41.93
T10					
D11			4.73	53.06	38.11
L12	7.42	122.73	4.66	55.13	43.39
S13	9.02	120.76	4.26	56.88	65.89
F14	8.37	119.91	5.51	56.76	39.93
V15	9.10	117.81	4.68	58.87	36.89
D16	8.52	116.85	4.18	54.55	38.91
I17	8.15	118.60	4.15	63.18	37.76
T18	8.73	122.16	4.91	60.57	70.60
D19	8.45	115.59	4.47	54.87	40.43
S20	8.12	108.50	4.61	57.66	66.09
S21	7.52	116.58	5.23	56.73	66.73
I22	8.21	113.85	4.48	60.32	42.65
G23	8.29	112.95	3.87	44.11	
L24	8.81	123.74	4.81	53.93	42.47
R25	8.57	119.98	4.89	54.04	33.85
W26	7.96	122.48	4.84	56.79	31.46
T27	9.76	119.81	4.75	60.69	68.46
P28			4.46	63.26	31.98
L29	8.52	124.21	4.49	54.14	43.04
N30	8.62	119.95	4.70	53.57	38.34
S31	8.09	114.28	4.55	57.50	63.48

S32			4.55	58.14	63.72
T33	8.00	114.15	4.29	63.62	69.53
I34	7.98	121.09	4.30	61.92	38.08
I35	8.81	126.23	4.21	61.72	38.78
G36			3.99	45.51	
Y37	7.30	120.40	5.07	57.93	38.95
R38			5.14	54.50	31.53
I39	9.04	129.56	5.06	60.27	40.78
T40	8.88	120.43	5.21	61.13	71.09
V41	8.82		5.02	61.28	33.80
V42	9.10	127.67	4.65	60.32	35.80
A43	9.41	131.34	4.41	52.41	18.75
A44	8.25	126.04	4.11	53.79	18.68
G45	8.70		4.12	45.62	
E46	8.11	119.65	4.46	55.87	30.52
G47	8.40		4.12	45.91	
I48	7.44	120.01	4.62	58.50	39.40
P49			4.53	63.59	31.88
I50	8.72	122.12	4.15	63.31	38.02
F51			4.76	57.90	41.86
E52			5.35	55.13	32.03
D53	8.84	122.75	4.99	52.95	44.77
F54	8.77	121.10	5.38	56.18	42.10
V55	8.28	125.76	4.32	59.14	34.94
D56	8.46	127.09	4.56	54.98	42.73
S57	8.25	119.63	4.33	60.63	62.68
S58	9.07	117.02	4.40	60.43	63.69
V59	7.57	119.35	3.79	65.66	32.39
G60	6.12	104.07	3.38	44.43	
Y61	6.08	117.69	5.03	56.31	41.69
Y62	8.44	126.64	4.44	58.56	43.55
T63	7.37	122.15	4.77	61.61	69.81

V64	8.86	127.94	3.66	61.84	31.84
T65	7.29	116.14	4.64	59.47	71.16
G66	8.45	105.56	3.99	45.86	
L67	7.85	119.08	4.18	53.38	41.63
E68	8.49	120.03	4.92	52.51	31.04
P69			4.47	62.74	31.41
G70	8.49	106.94	4.06	45.83	
I71	7.50	120.07	4.08	58.71	40.41
D72	8.19	124.92	4.93	54.25	41.12
Y73	9.30	122.43	5.06	57.38	40.55
D74	9.29	122.98	5.21	53.89	42.12
I75	8.80	124.27	5.47	58.40	40.89
S76	8.76	121.29	5.80	56.34	66.18
V77	9.42	124.74	4.76	61.19	33.27
I78	9.36	126.30	4.71	61.16	41.05
T79	8.55	122.35	4.28	64.26	69.13
L80	8.66	128.89	4.73	54.06	41.47
I81	8.34	121.64	4.86	59.30	40.51
N82	8.81	123.24	4.64	53.45	38.94
G83	8.63	112.67	4.00	45.42	
G84	8.28	108.56	3.97	45.19	
E85	8.45	120.69	4.31	56.48	30.48
S86	8.34	116.86	4.42	57.92	63.72
A87	8.24	126.89	4.58	50.45	18.10
P88			4.47	62.96	31.46
T89	8.27	114.27	4.34	62.32	69.53
T90	8.09	116.29	4.33	61.89	69.50
L91	8.28	124.66	4.40	55.58	41.60
T92	8.09	115.29	4.30	61.89	69.50
Q93	8.38	123.20	4.35	55.72	29.05
Q94	8.47	122.72	4.39	55.78	29.10
T95	7.83	121.20	4.40	63.17	70.40

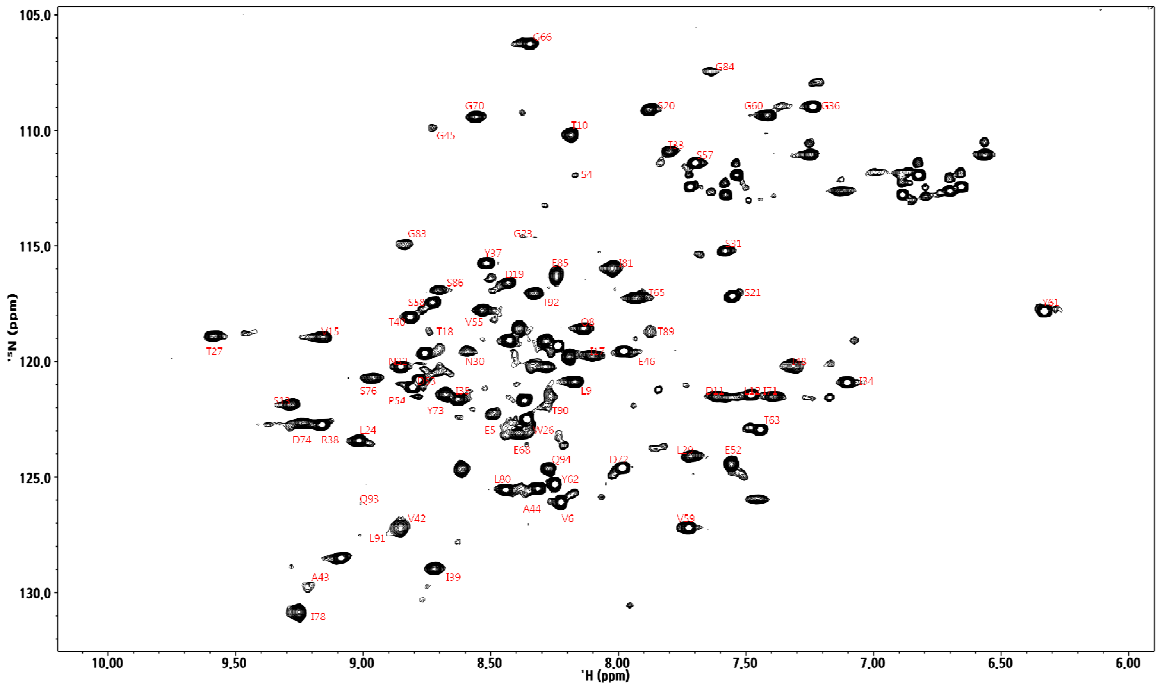

Figure 16. 2D ^{1}H-^{15}N HSQC spectrum of EDB in the free state with assignment

80 % assigned 2D ^{1}H-^{15}N HSQC spectrum of EDB-aptide complex in sodium phosphate buffer, pH 6.0. The spectrum was acquired at 900 MHz, 298 K, in 20 mM NaPi buffer at pH 6.0 containing 0.01 % NaN_3. This drawing was made using the NMRViewJ program.

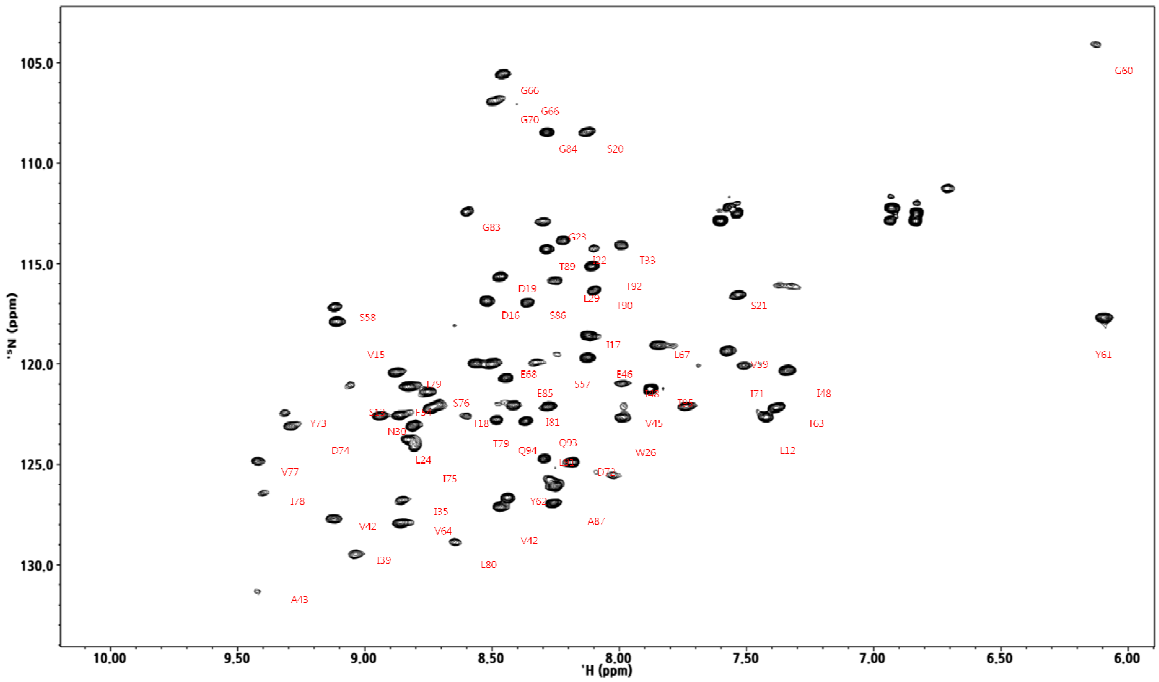

Figure 17. 2D ^{1}H-^{15}N HSQC spectrum of EDB in complex with aptide

97 % assigned 2D ^{1}H-^{15}N HSQC spectrum of EDB in sodium phosphate buffer, pH 6.0. The spectrum was acquired at 900 MHz, 298 K, in 20 mM NaPi buffer at pH 6.0 containing 0.01 % NaN_3. This drawing was made using the NMRViewJ program.

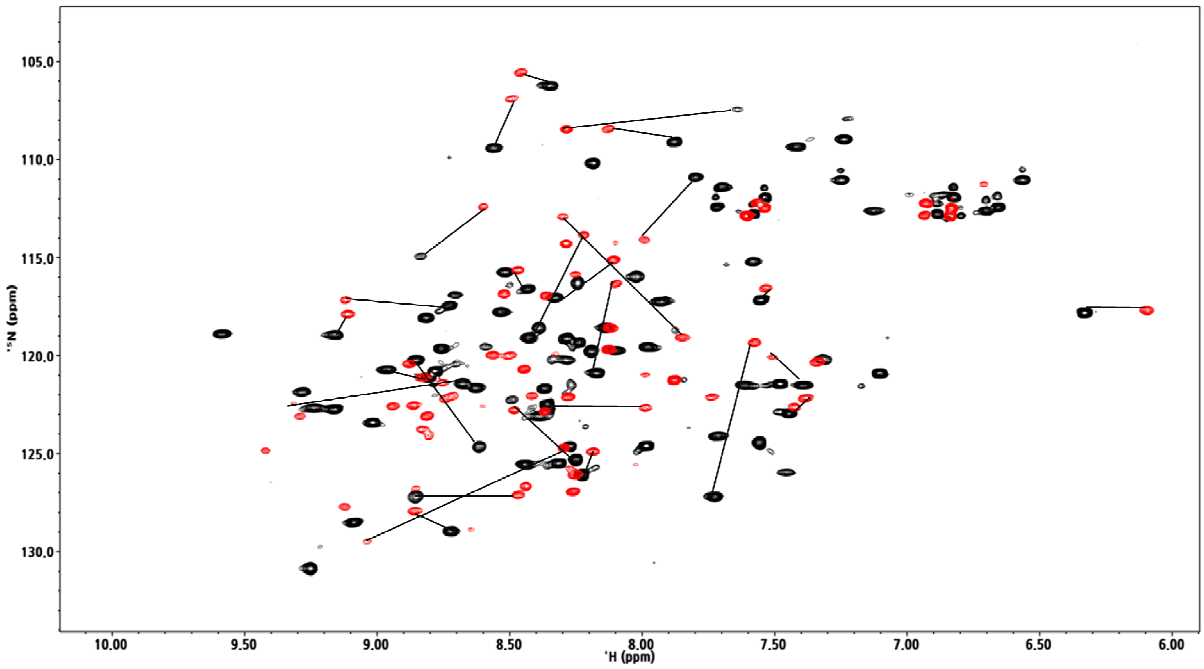

Figure 18. Chemical shift mapping of aptide bind to the EDB.

Overlay of 2D $^{1}H–^{15}N$ HSQC spectra of EDB recorded in the absence (in black) and presence (in red). The spectrum was acquired at 900 MHz, 298 K, in 20 mM NaPi buffer at pH 6.0 containing 0.01 % NaN_3. This drawing was made using the NMRViewJ program.

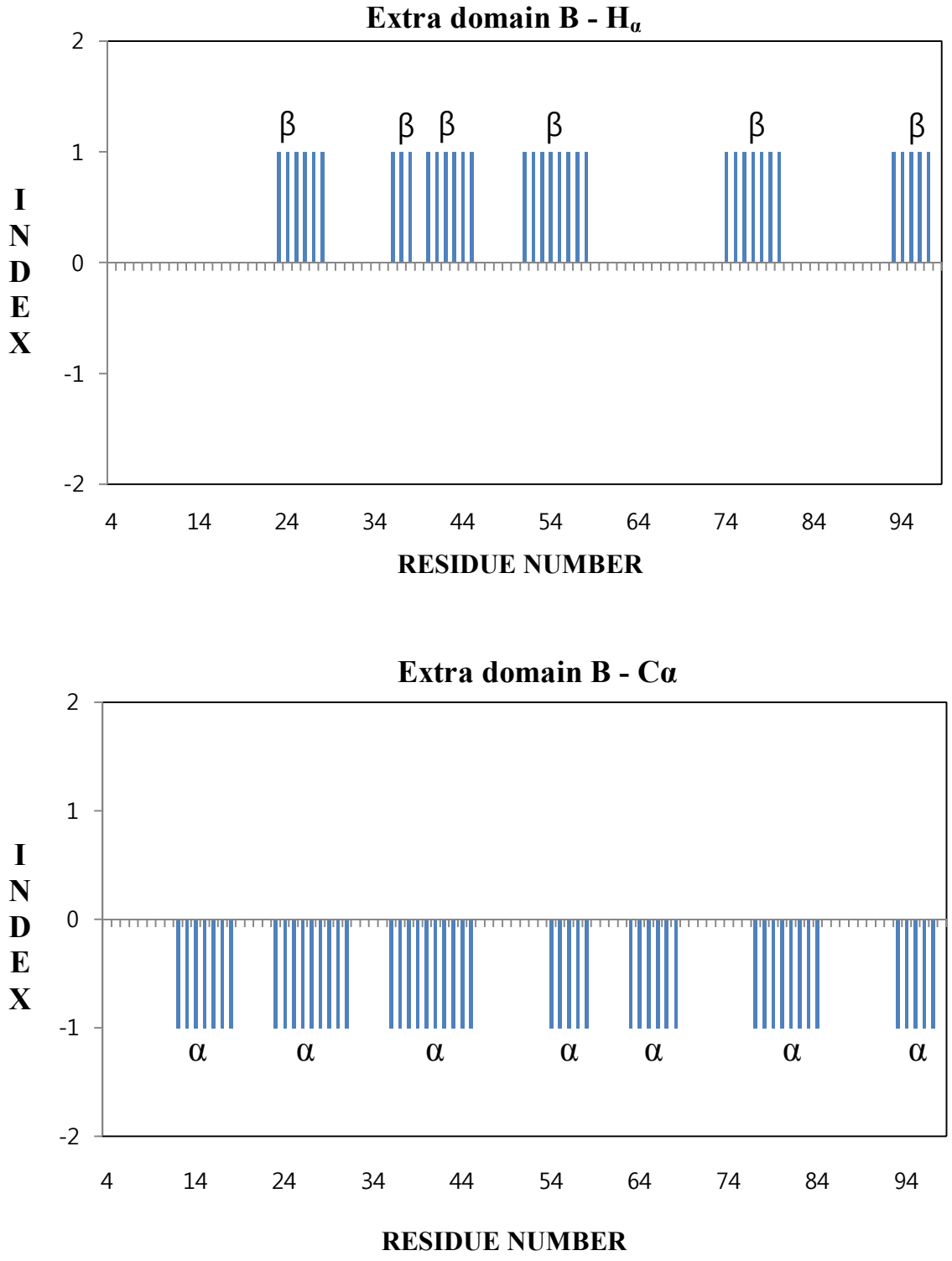

Figure 19. Chemical shift index (Hα, Cα) plot of EDB in the free state

The chemical shift index is plotted for α-^{1}H resonance assignment (top) and α-^{13}C resonance assignments (bottom)

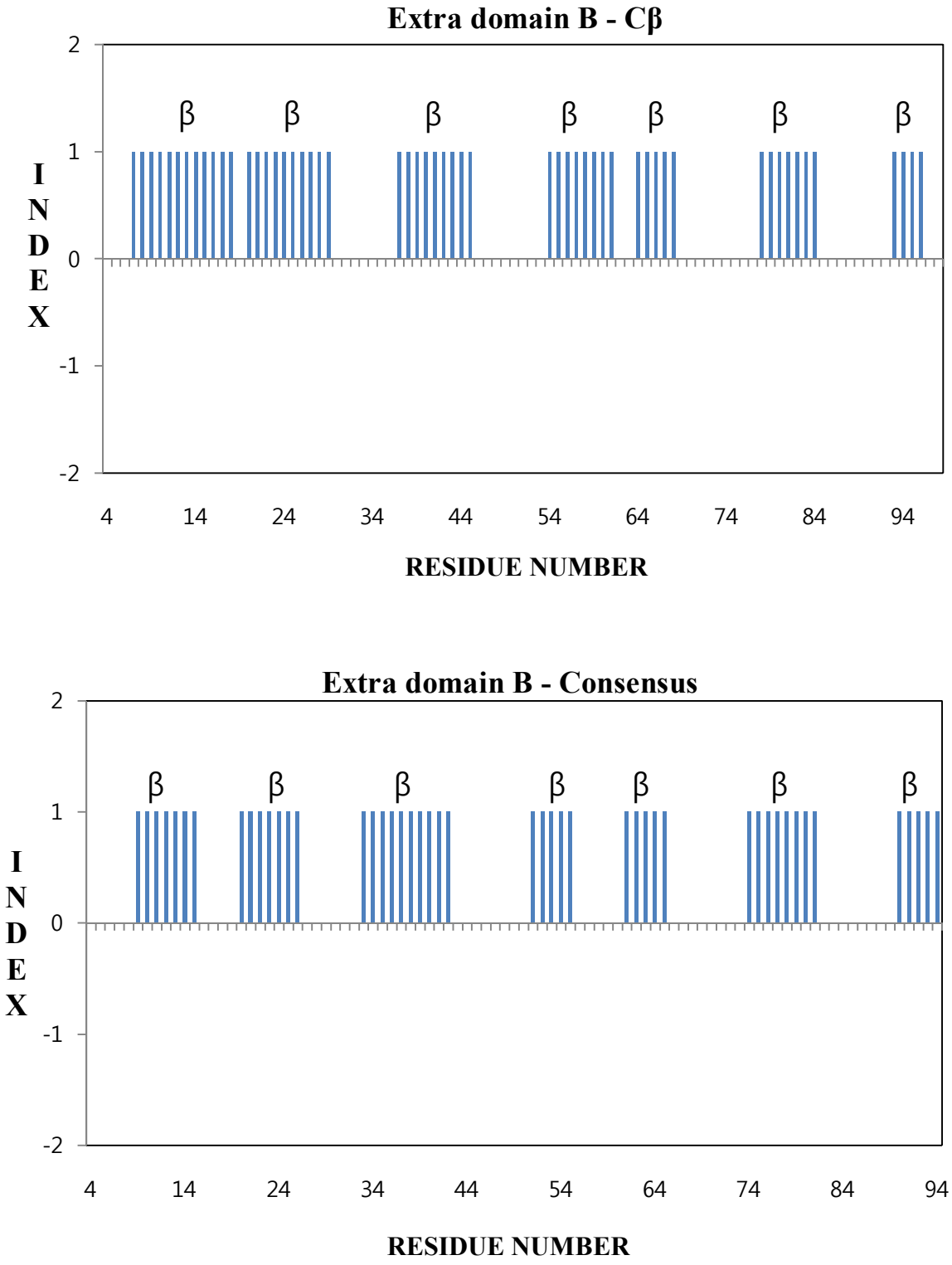

Figure 20. Chemical shift index (C_β, consensus) plot of EDB in the free state

The chemical shift index is plotted for β-^{13}C resonance assignment (top) and consensus resonance assignments (bottom)

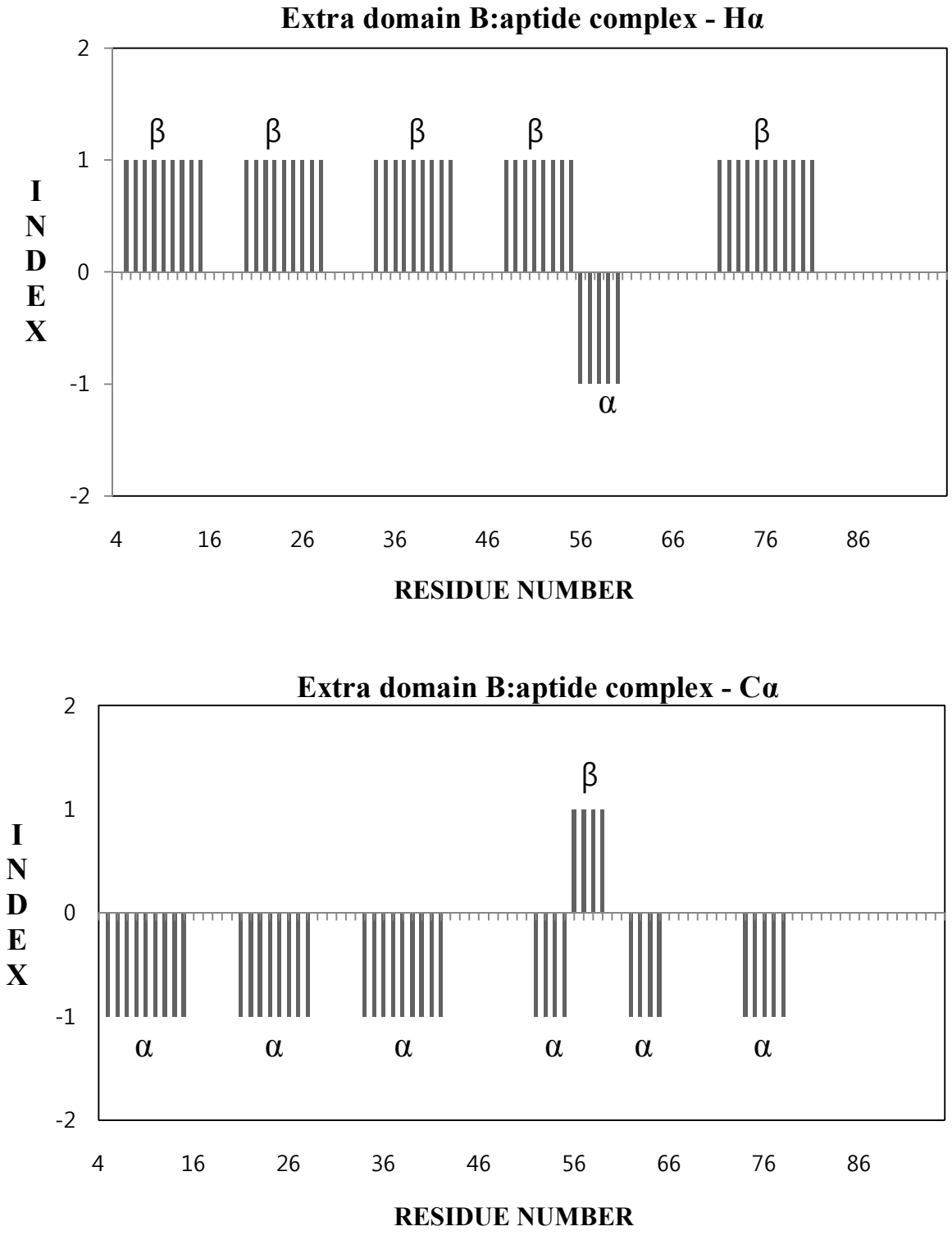

Figure 21. Chemical shift index plot for EDB:aptide complex: Hα, Cα

The chemical shift index is plotted for α-^{1}H resonance assignment (top) and α-^{13}C resonance assignments (bottom)

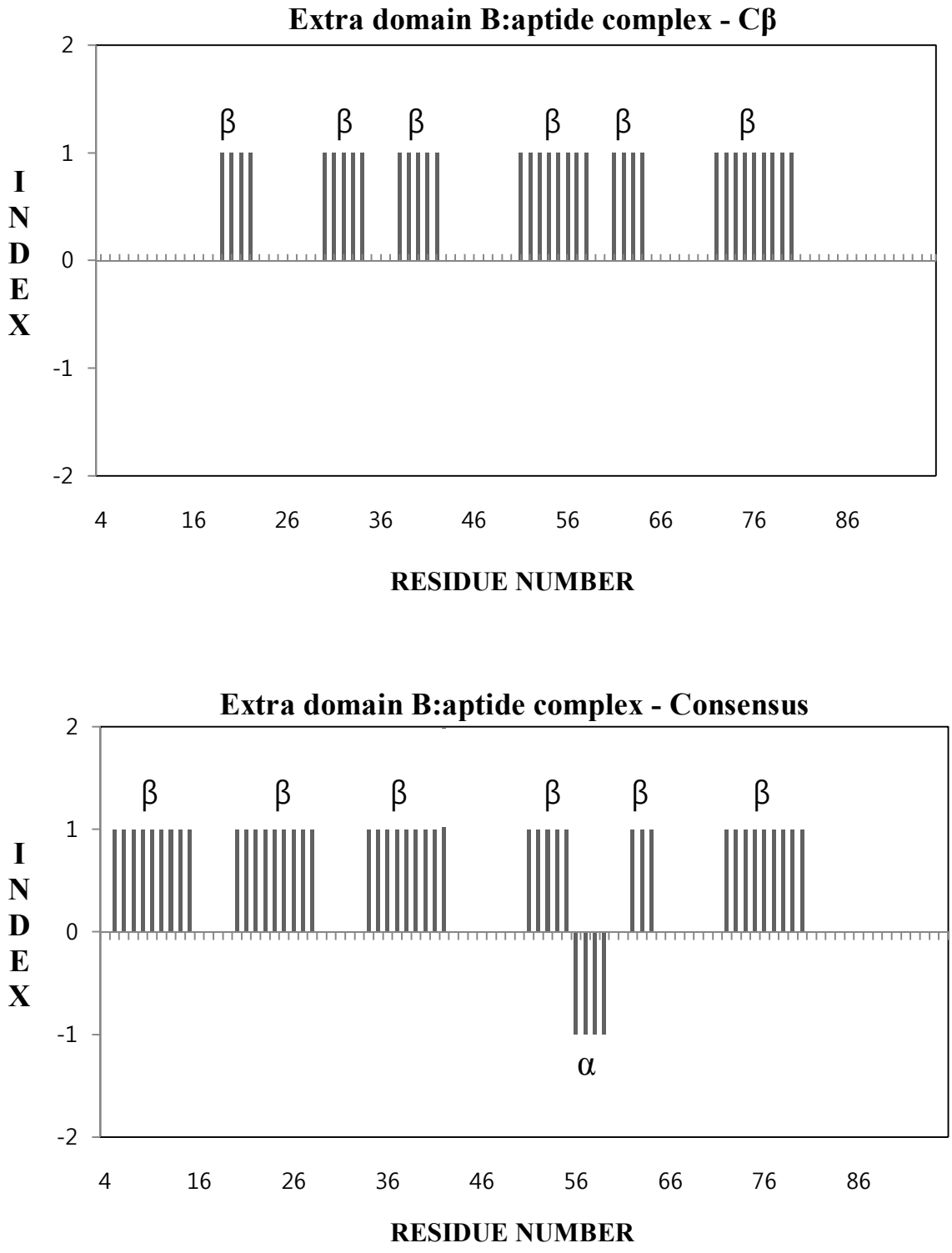

Figure 22. Chemical shift index plot for EDB:aptide complex: Cβ, consensus

The chemical shift index is plotted for β-^{13}C resonance assignment (top) and consensus resonance assignments (bottom)

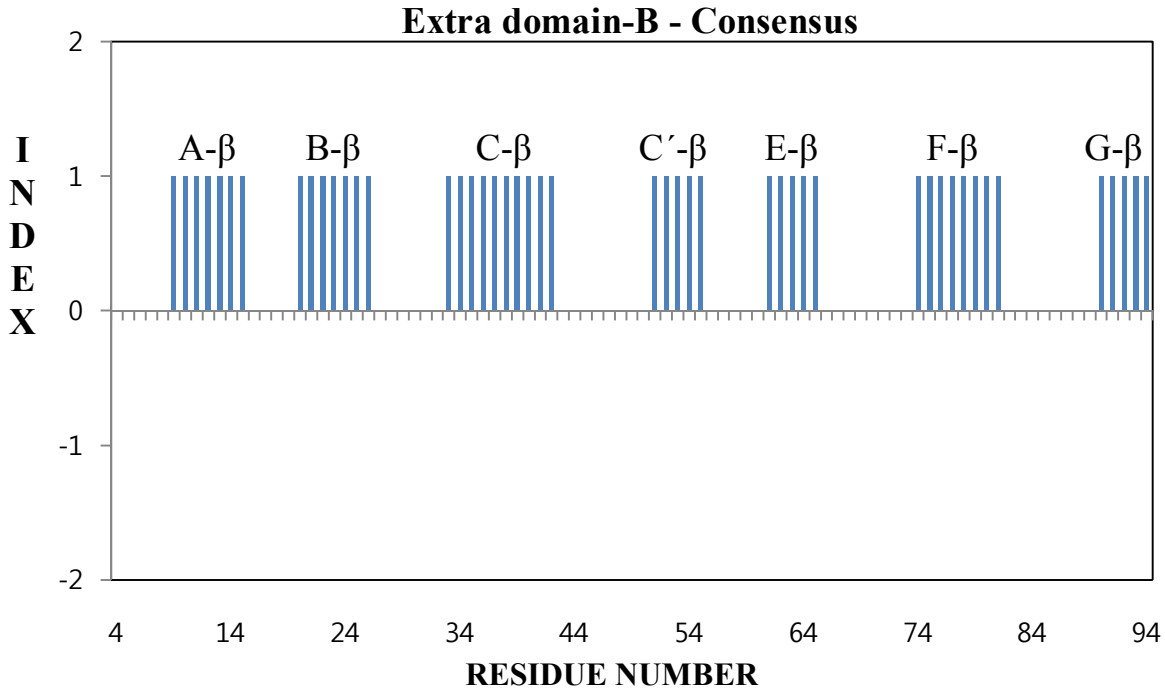

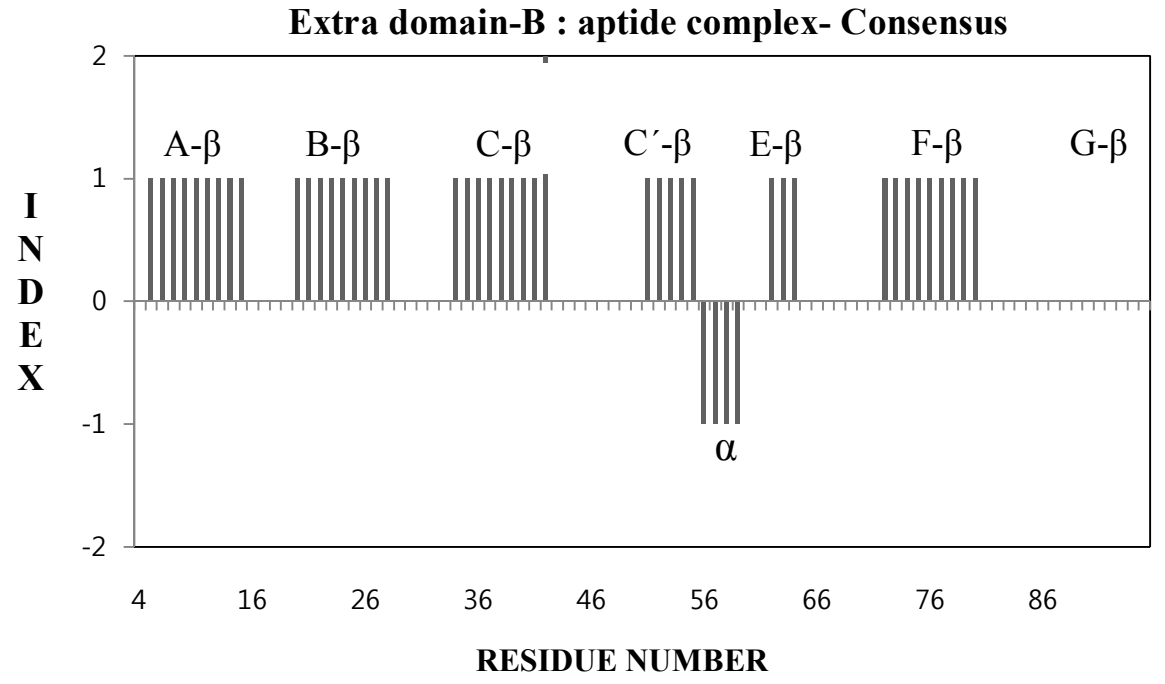

Figure 23. Chemical shift index plot for EDB and EDB:aptide complex

Ⅳ. CONCLUSION

The complex of fibronectin extra domain B and its specific binding aptide has been investigated by multidimensional heteronuclear NMR spectroscopy. A nearly complete set of backbone chemical shift assignments (~97%) of the EDB:aptide complex was obtained by 3D CBCACONH, HNCACB, and HBHACONH experiments using double labeled ($^{13}C/^{15}N$) and triple labeled ($^{2}H/^{13}C/^{15}N$) NMR samples. The $^{1}H\alpha$, $^{13}C\alpha$, and $^{13}C\beta$ resonance assignment enabled the secondary structure calculation of the EDB:aptide complex by the Chemical Shift Index (CSI) analysis. The CSI results indicated that six β-strand secondary structures were found between residues 5-15, 20-28, 34-42, 51-55, 62-64, and 72−80 and also an α-helical turn between residues 56−59.

Comparison of the CSI between free EDB and the EDB:Aptide complex revealed the changes in the secondary structures during the complex formation. The backbone assignment in this study combined with the side chain assignment will provide crucial information to calculate the three-dimensional complex structure. Experiments to collect structural information such as distance restraints (NOE), dihedral angle restraints (J coupling), and the orientational restraints (RDC) are underway.

Ⅴ. REFERENCES

Andrea G. Cochran, Nicholas J. Skelton, and Melissa A. Starovasnik. 2001. Tryptophan zippers: Stable, monomeric β-hairpins. Proc Natl Acad Sci U S A. 98:10 5578-5583.

Alessi P, Ebbinghaus C, Neri D. 2004. Molecular targeting of angiogenesis., Biochem Biophys Acta.;1654:39-49.

Carnemolla B BE, Siri A, Zardi L, Nicotra MR, Bigotti A, Natali PG. 1989. A tumor-associated fibronectin isoform generatied by alternative splicing of messenger RNA precursors. J Cell Biol.108:1139-48.

Chames P, Van Regenmortel M, Weiss E, Baty D. 2009. Therapeutic antibodies: successes, limitations and hopes for the future. Br J Pharmacol.;157;220-33.

Delaglio F, Grzesiek S, Vuister G W, G. Zhu, J. Pfeifer, A. Bax. 1995. NMRPipe: a multidimensional spectral processing system based on UNIX pipe. J. Biomol.NMR. 277-293

Clore G Marius, Gronenborn Angela M. 1998. NMR structure determination of proteins and protein complexes larger than 20 kDa, Chemical Biology. 2:564–570.

Ebbinghaus C, Scheuermann J, Neri D, Elia G. 2004. Diagnostic and therapeutic

applications of recombinant antibodies: targeting the extra-domain B of fibronectins, a marker of tumor angiogenesis. Curr Pharm Des.10;1537-49

Fattorusso Roberto, Maurizio Pellecchia, Francesca Viti, Neri, Paolo, Neri, Dario; and Wuthrich, Kurt. 1999. NMR Structure of the Angiogenesis Marker Oncofoetal Fibronectin ED-B Domain. Cell Structure 7, 381-390.

Garrett, D.S., Powers, R., Gronenborn, A.M. & Clore, G.M. 1991. A common sense approach to peak picking two-, three- and four-dimensional spectra using automatic computer analysis of contour diagrams. J. Magn. Reson. 95, 214-220

Grezesiek S, Bax, A. 1993. Amio-acid type determination in the sequential assignment procedure of Uniformly C-13/N-15-enriched proteins. Journal of Biomolecular NMR. 185-204

Gutman A, Kornblihtt AR. 1987. Identification of a third region of cell-specific alternative splicing in human fibronectin mRNA, Proc Natl Acad Sci USA. 84:7170-82.

Higman, V. A., Watts, A, Clore, M., Potts, J. 2012. Recent Developments in Biomolecular NMR. The Royal Society of Chemistry. 318-334.

Hynes RO, Kreis T. and Vale R., eds. Sambrook and Tooze Publishers. 1999. Fibronectins. in: Guidebook to the Extracellular Matrix, Anchor and Adhesion Proteins. Oxford University Press. 422-425.

Jean E. Schwarzbauer. 1991. Alternative splicing of fibronectin: three variants, three functions. Bioessays.13:527-33.

Johnson BA, Blevins RA. 1994. NMR View: A computer program for the visualization and analysis of NMR data. J Biomol NMR. 603-14.

Kaczmarek J CP, Nicolo G, Spina B, Allemanni G, Zardi L. 1994. Distribution of oncofeteal fibronectin isoforms in normal, hyperplastic and neoplastic hyman breast tissues. Int J Cacncer. 59:11-16.

Kaspar M, Zardi L, Neri D. 2006. Fibronectin as target for tumor therapy. Int J cancer. 118:1331-9.

Khan ZA, Chan BM, Uniyal S, Barbin YP, Farhangkhoee H, Chen S. 2005. EDB fibronectin and angiogenesis – a novel mechanistic pathway. Angiogenesis.8:183-96.

Kim S BK, Mousa SA and Varner JA. 2000. Regulation of angiogenesis in vivo by ligation of integrin a5bs1 with the central cell-binding domain of fibronectin. Am J

Pathol. 156:1345-62.

Kim Sunghyun, Kim Daejin, Jung Hyun Ho, Lee In-Hyun, Prof. Kim Jae IL, Suh Jeong-Yong, Jon Sangyong. 2012. Bio-inspired design and potential biomedical applications of a novel class of high-affinity peptides. Angewandte Chemie.51;1890-4.

Montalvao RW, Cavalli A, Salvatella X, Blundell TL, Vendruscolo M. 2008. Structure determination of protein-protein complexes using NMR chemical shifts: case of an endonuclease colicin-immunity protein complex, J Am Chem Soc. 26;130:15990-6.

Nietlispach D, H.R. Mott, K.M. Stott, P.R. Nielsen, A. Thiru and E.D. Laue. 2008. Structure Determination of Protein Complexes by NMR, University of Cambridge.

NI Kirby, EF DeRose, RE London, GA Muelle.r. 2004. NvAssign: protein NMR spectral assignment with NMRView. Bioinformatics. 20; 1201-1203.

Oyama F HS, Shimosato Y, Titani K, Sekiguchi K.. 1989. Deregulation of alternative splicing of fibronectin pre-mRNA in malignant human liver tumors. J Biol Chem. 264:10331-4.

Oyama F HS, Shimosato Y, Titani K, Sekiguchi K. 1990. Oncodevelopmental regulation of the alternative splicing of fibronectin premessenger RNA in human lung

tissues. Cancer Res. 50:1075-8.

Pankov R, Yamada KM. 2002. Fibronectin at a glance. J Cell Sci. 15;115:3861-3.

Park J, Kim S, Saw PE, Lee IH, Yu MK, Kim M, et al. 2012. Fibronectin extra domain B-specific aptide conjugated nanoparticles for targeted cancer imaging. J Control Release. 163;111-8

Pupa SM MS, Forti S, Tagliabue E. 2002. New insights into the role of extracellular matrix during tumor onset and progression, J Cell Physiol. 192:259-67.

Saw Phei Er, Kim Sunghyun, Lee In-hyun, Park Jinho, Yu Mikyung, Lee Jinju, Kim bae-Il and Jon Sangyong. 2013. Aptide-conjugated liposome targeting tumor-associated fibronectin for glioma therapy. J. Mater. Chem. B, ,1, 4723-4726

Schwarzbauer JE PR, Fonda D, Hynes RO. 1987. Multiple sites of alternative splicing of the rat fibronectin gene transcript. EMBO J. 6:2573-80.

Weiss, A, den Bergh H, Griffioen AW, Nowak-Sliwinska P. 2012. Angiogenesis inhibition for the improvement of photodynamic theraphy: the revival of a promising idea. Biochim Biophys Acta. 1826:53-70.

Wernert N. 1997, The multiple roles of tumour stroma. Virchows Arch. 430:-43.

Wittekind, M, Mueller, L. 1993. HNCACB, a high-sensitivity 3D NMR experiment to correlate amide-proton and nitrogen resonances with the α- and β-carbon resonances in proteins. J. Magn. Reson. B.101:201-205.

Wishart David S., Sykes BD and Richards FM. 1991. Relationship between nuclear magnetic resonance chemical shift and protein secondary structure, Journal of Molecular Biology. 222: 311-333.

Wishart David S.,. Sykes B D , Richards F M. 1992. The chemical shift index: a fast and simple method for the assignment of protein secondary structure through NMR spectroscopy. Biochemistry. 31: 1647–1651

Wishart David S., Brian D. Sykes. 1994. The 13C Chemical-Shift Index: A simple method for the identification of protein secondary structure using 13C chemical-shift data. Journal of Biomolecular NMR. 4:2 171-180.

Yingxi Lina,b and Gerhard Wagnera. 1999. Efficient side-chain and backbone assignment in large proteins: Application to tGCN5, Journal of Biomolecular NMR. 227–239.

국문 초록

혈관 생성 시 발생하는 표지 단백질인 파이브로넥틴 EDB는 주로 악성고체종양에서 발현되며 정상적인 혈관과 조직에서는 발견되지 않는다고 보고되어 있다. 이로부터 EDB를 표적으로 하여 종양 진단 및 치료제를 개발하기위한 연구가 활발하게 이루어지고 있다. 그 중 항체와 같이 표적물질에 높은 친화도와 특이성을 가지고 결합할 수 있는 저분자 펩타이드인 앱타이드가 개발되었는데, β-hairpin 골격의 양 말단에 표적을 인식하는 두 개의 펩타이드 다리가 연결된 구조로 되어 있다. EDB에 대하여 선별된 앱타이드는 in vitro와 in vivo 모두 높은 반응성을 보였는데,저분자 물질이 가지는이와 같은 높은 결합력과 특이성을 분자수준에서 이해하기 위해서는 EDB-앱타이드 복합체의 삼차원 구조가 필수적이다. 본 논문에서는 NMR 구조 결정을 위하여 EDB 및 EDB-앱타이드 복합체의 backbone assignment를 수행하였다.

^{2}H, ^{13}C, ^{15}N과 같은 안정 동위원소로 표지한 EDB를 발현하여 정제하였고,CBCA(CO)NH, HNCACB 그리고 HBHA(CO)NH와 같은 삼차원 핵자기공명 실험을 수행하였다. Sequential assignment 방법을 이용하여 단백질 backbone assignment를 한 결과,EDB 복합체의 경우97%의 $^{1}H\alpha$, $^{13}C\alpha$,$^{13}C\beta$의 chemical shift assignment를 완성하였다. Chemical Shift Index (CSI)를 이용하여 단백질의 2차 구조를 예측한 결과, EDB에서는 7

개의 β-strand가 있는 반면, EDB 복합체에서는 6개의 β-strand와 한 개의 α-helical turn구조를 가지는 것을 알 수 있었다. 이는 EDB가 앱타이드와 복합체를 형성하는 과정에서 2차 구조가 두드러지게 변화하는 것을 의미한다.

본 논문에서 얻어진 backbone assignment를 기반으로 향후 side chain assignment를 완성하고 distance restraint를 측정하여 EDB 복합체의 삼차원 구조를 계산할 예정이다. 복합체구조 및 결합 양태에 대한 연구 결과는 바이오마커, 의약물질, 그리고 약물전달체로서 앱타이드의 가능성을 현실화 하는 데에 크게 기여할 것으로 예상한다.

.....

주요어: 앱타이드, backbone assignment, 파이브로넥틴 extra domain B(EDB) 핵자기공명분광법, 단백질상호작용

학번 : 2012-22623